BRAIN RESEARCH 1410 (2011) 12-23

available at www.sciencedirect.com

ScienceDirect

www.elsevier.com/locate/brainres

BRAIN RESEARCH

Research Report

Astrocytic neuroprotection through induction of cytoprotective molecules; a proteomic analysis of mutant P301S tau-transgenic mouse

Kenichiro Yata[a,*], *Shinji Oikawa*[b], *Ryogen Sasaki*[a], *Akihiro Shindo*[a], *Rong Yang*[c], *Mariko Murata*[b], *Kenji Kanamaru*[d], *Hidekazu Tomimoto*[a]

[a]*Department of Neurology, Mie University Graduate School of Medicine, Tsu 514-8507, Japan*
[b]*Department of Environmental and Molecular Medicine, Mie University Graduate School of Medicine, Tsu 514-8507, Japan*
[c]*Department of Physiology, Nanjing Medical University, Nanjing 210029, China*
[d]*Departmento of Neurosurgery, Suzuka Kaisei Hospital, Suzuka 513-0836, Japan*

ARTICLE INFO

Article history:
Accepted 29 June 2011
Available online 7 July 2011

Keywords:
Tauopathy
Astrocyte
Heat shock protein 27
Peroxiredoxin 6
Apolipoprotein E
Latexin

ABSTRACT

Hyperphosphorylated tau protein constitutes a significant portion of intracellular inclusions in some neurodegenerative diseases. In addition, mutations in tau protein cause familial forms of frontotemporal dementia (FTD), indicating that dysfunction of tau protein is responsible for neurodegeneration and dementia. P301S tau-transgenic (Tg) mouse expressing human mutant tau in neurons exhibits similar features of human tauopathies including neuronal degeneration and filament accumulation consisted of hyperphosphorylated tau protein. In the present study, we attempted to characterize protein expression profiles in P301S tau-Tg mouse by using two-dimensional differential in-gel electrophoresis (2D-DIGE) coupled by peptide mass fingerprinting (PMF). As a result, we identified four upregulated proteins; heat shock protein 27 (Hsp27), peroxiredoxin 6 (Prdx6), apolipoprotein E (ApoE), and latexin (LTXN), all of which may function as a neuroprotective mechanism against tau toxicity. In immunohistochemistry, these four proteins were increased invariably in astrocytes, and these astrocytes infiltrated the area in which there are numerous accumulations of hyperphosphorylated tau and neuronal loss. Therefore, these results may indicate that astrocytes provide a neuroprotective mechanism against tau toxicity.

1. Introduction

Tau is one of the microtubule-associated proteins which play an important role in regulating microtubule assembly and stabilization, as well as maintenance of axonal transport. Under pathological conditions, tau becomes hyperphosphorylated, and is dissociated from microtubules and subsequently assembled into abnormal filaments. Tauopathy, a neurodegenerative

* *Corresponding author at:* Department of Neurology, Mie University Graduate School of Medicine, Edobashi 2-174, Tsu, 514-8507, Japan. Fax: +81 59 231 5212.
E-mail address: ken-yata@mbk.nifty.com (K. Yata).

Abbreviations: FTDP-17, frontotemporal dementia with parkinsonism linked to chromosome 17; 2D-DIGE, two-dimensional differential in-gel electrophoresis; PMF, peptide mass fingerprinting; Hsp27, Heat shock protein 27; Prdx6, Peroxiredoxin 6; ApoE, Apolipoprotein E; LTXN, Latexin; GFAP, glial fibrillary acidic protein; AD, Alzheimer's disease

0006-8993/$ – see front matter © 2011 Elsevier B.V. All rights reserved.
doi:10.1016/j.brainres.2011.06.064

disorder characterized by tau inclusions, refers to a group of increasingly recognized, adult-onset, progressive neurodegenerative diseases, including Pick's disease, progressive supranuclear palsy, corticobasal degeneration and frontotemporal dementia with parkinsonism linked to chromosome 17 (FTDP-17) (Kosik and Shimura, 2005; Lee et al., 2001). Discovery of over 30 tau gene mutations responsible for FTDP-17 clearly indicates that tau abnormalities are pivotal in neurodegeneration (Iqbal et al., 2009; Tsuboi, 2006); however, the molecular mechanisms leading to neuronal dysfunction and death remained unclear.

Tau-transgenic (Tg) mouse provides an experimental tool for defining relationships between tau mutation and neurodegeneration (Trojanowski et al., 2002). Such a model is also invaluable for developing new diagnostics and therapeutic strategy for tauopathies in humans. P301S tau-Tg mouse expressing human mutant tau in neurons exhibits an essential feature of tauopathies, including neurodegeneration and filamentous accumulation consisted of hyperphosphorylated tau protein (Allen et al., 2002; Baba et al., 2007; Bellucci et al., 2004; Delobel et al., 2008; Yoshiyama et al., 2007). This mouse exhibits numerous tau-positive neurons in the brainstem and spinal cord, and less numerously in the other brain regions including the cerebral cortex and hippocampus (Allen et al., 2002). In addition, the mouse exhibits neurological phenotypes dominated by severe paraparesis, possibly due to loss of the anterior horn cells in the spinal cord. Therefore, in the present study, we sought to identify possible alteration of protein levels related to tau mutation in the spinal cord by using two-dimensional differential in-gel electrophoresis (2D-DIGE) followed by peptide mass fingerprinting (PMF), and cellular source of these proteins by immunohistochemistry.

2. Results

2.1. *Proteomic analysis reveals differentially-expressed proteins in P301S tau transgenic mouse by 2D-DIGE*

Individual spin protein extracts from P301S tau-Tg (n=4) and wild (Wt) (n=4) mice were compared using the 2D-DIGE technique. Fig. 1A shows a representative 2D-DIGE image with spot numbers. The number of protein spots was estimated to be 1586. 2D-DIGE analyses were processed using DeCyder Differential Analysis Software (GE healthcare), which was designed specifically for 2D-DIGE experiments. 2D-DIGE analyses rendered 32 spots that exhibited statistically significant changes in their expression level between P301S tau-Tg and Wt mice (Student's t-test, $p<0.05$).

2.2. *Identification of differentially expressed proteins*

As shown in Table 1, the 32 differentially expressed spots were identified successfully as 25 proteins by PMF. We focused on any protein that showed more than a 1.5-fold difference in protein level between P301S tau-Tg and Wt samples. As a result, glial fibrillary acidic proteins (GFAPs) and four intriguing proteins were detected (spot number 1197: apolipoprotein E (ApoE), spot number 1274: latexin (LTXN), spot number 1339: heat shock protein 27 (Hsp27), and spot number 1342: peroxiredoxin-6 (Prdx6)). Figs. 1B–E shows these four selective spots showing more than a 1.5-fold difference protein level between P301S tau-Tg and Wt mice.

2.3. *Upregulation of the four proteins in P301S tau-Tg mouse by western blotting*

Spin protein samples from P301S tau-Tg (n=5) and Wt (n=5) mice were analyzed by western blotting to estimate their content of four proteins (Hsp27, Prdx6, ApoE, LTXN). The intensity of the β-actin signal was similar between two groups and was, therefore, used as an internal reference for cross-sample normalization. Fig. 2A shows a representative western blot of the four proteins. The intensity of the bands of four proteins was stronger in samples from P301S tau-Tg mice than in those from Wt mice. Upon quantification, the signal intensities of Hsp27, Prdx6, ApoE, and LTXN, were 2.8-fold, 2.1-fold, 1.4-fold, and 1.5-fold higher, respectively, in P301S tau-Tg mice than in Wt mice.

2.4. *Astrocyte activation and neuronal loss in the anterior horn of the spinal cord in P301S tau-Tg mouse*

GFAP was detected as a significantly-upregulated protein in P301S tau-Tg mouse after proteomics analysis. Thus, we performed immunostaining of GFAP in the spinal cord of P301S tau-Tg and Wt mouse (Figs. 3A–D). In Wt mouse, GFAP-positive astrocytes were distributed numerously in the white matter, and much less in the gray matter (Fig. 3A: low magnification, C: high magnification in the anterior horn). On the contrary, in P301S tau-Tg mouse (Fig. 3B: low magnification, D: high magnification in the anterior horn), these astrocytes were present in the both gray and white matters, but prominently in the anterior horn (arrow in Fig. 3B). Figs. 3E and F shows hematoxylin and eosin (HE) staining of the anterior horn of Wt and P301S tau-Tg mouse, respectively. Swollen or atrophic motor neurons were observed in P301S tau-Tg mouse.

To identify the relationship between tau accumulation and astrocyte infiltration, we compared the localization of AT8 and GFAP positive structures. In P301S tau-Tg mouse (Fig. 3G), most AT8 staining was localized to the anterior horn of the spinal cord. In a higher magnification, phosphorylated tau was accumulated in the neuronal perikarya and thread-like or punctuate structures in the neuropil (Fig. 3H). These tau-positive structures were also stained by Gallyas sliver stain (Fig. 3I). Double immunofluorescence histochemistry for GFAP (Fig. 3J), AT8 (Fig. 3K) further revealed absence of their colocalization (Fig. 3L). With immunohistochemistry for NeuN, neurons were obviously decreased in number in the anterior horn of the spinal cord (Fig. 3N: low magnification, 3P: high magnification of the anterior horn) in P301S tau-Tg mouse, compared to WT mouse (Fig. 3M: low magnification, 3O: high magnification of the anterior horn). Collectively, these data may indicate that tau accumulation led to astrocytic activation and neuronal loss.

2.5. *Upregulation of neuroprotective proteins in activated astrocytes*

To identify localization of the four upregulated proteins, we performed double immunostaining in the spinal cord of Wt and P301S tau-Tg mouse. Figs. 4A–D shows double

immunofluorescence histochemistry for Hsp27 and GFAP in the anterior horn. In P301S tau-Tg mouse (Figs. 4A–C), immunoreactivity for Hsp27 was colocalized with GFAP-immunoreactive astrocytes, but not in the neurons (arrow in Fig. 4C indicates absence of neuronal staining). On the contrary, in Wt mouse (Fig. 4D), immunoreactivity for Hsp27 was observed in the neurons of the anterior horn, but not in GFAP-immunoreactive astrocytes. Figs. 4E–H shows double immunofluorescence histochemistry for Hsp27 and GFAP in the white matter adjacent to the anterior horn. In P301S tau-Tg mouse (Figs. 4E–G), Hsp27 was obviously colocalized with GFAP in the astrocytic perikarya and their processes. Conversely, in Wt mouse (Fig. 4H), Hsp27 was expressed in the neuronal perikarya, but no staining was identified in their processes.

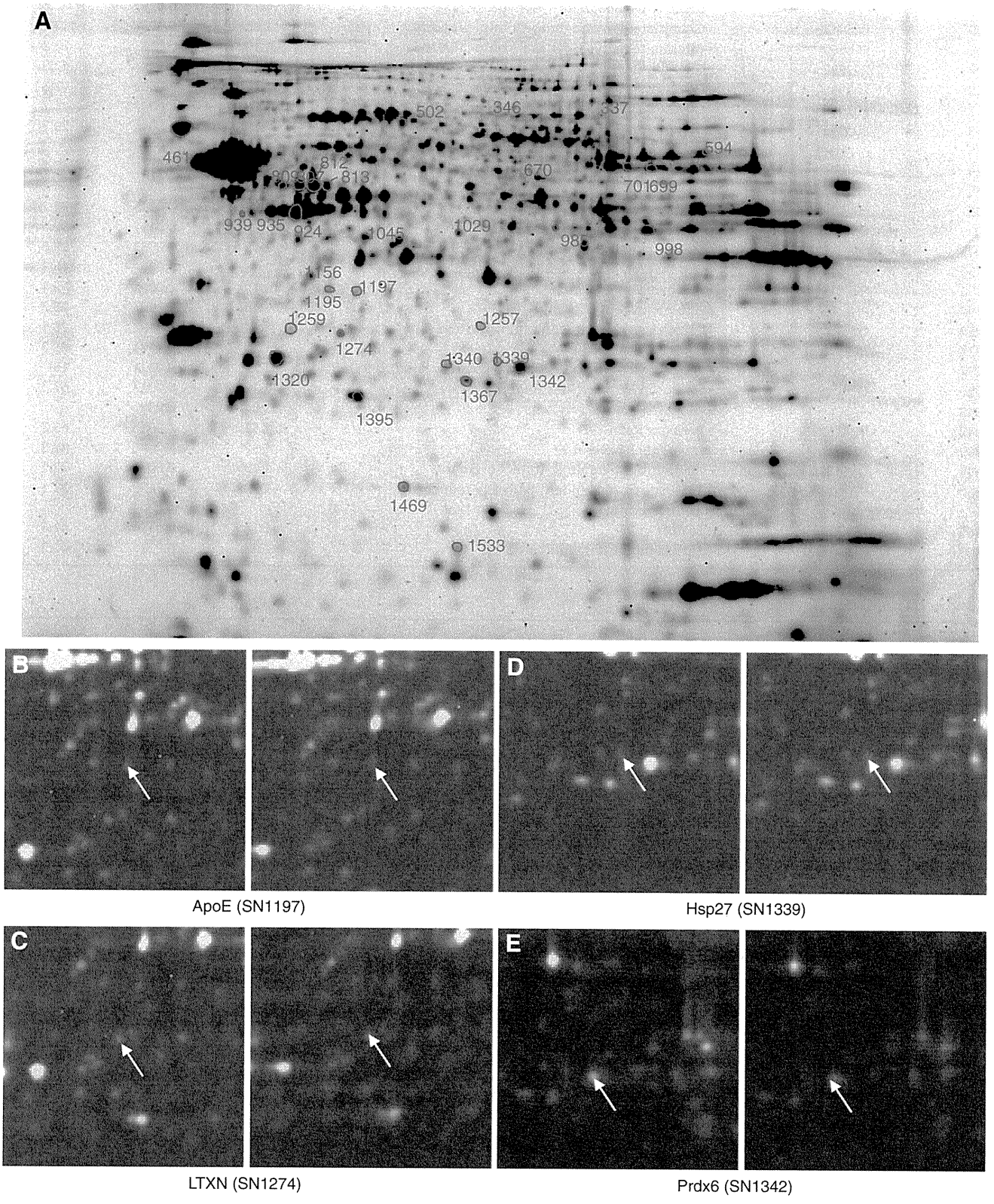

Table 1 – Proteins identified to be significantly regulated in P301S tau-Tg mouse.

Spot number	Accession number	Protein name	Fold difference	p-value[a]	Coverage[b]
337	Q921	Serotransferrin	1.4	0.005	9.3
346	P26040	Ezrin or Mitochondrial inner membran protein	1.14	0.028	12
461	P08551	Neurofilament light polypeptide OS	−1.43	0.00028	37.9
502	Q8BMF4	Dihydrolipoyllysine-residue acetyltransferase cmponent of pyruvate dehydrogenase complex	−1.12	0.019	17.9
594	P52480	Pyruvate kinase isozymes M1/M2	1.15	0.028	26.4
670	Q00612	Glucose-6-phosphate 1-dehydrogenase	1.19	0.016	21.6
699	P26443	Glutamate dehydrogenase 1 mitochondria	1.12	0.005	12.7
701	P10860	Glutamate dehydrogenase 1 mitochondria	1.13	0.043	23.8
807	P03995	Glial fibrillary acidic protein	1.72	0.012	42.3
812	P03995	Glial fibrillary acidic protein isoform 1	2.34	0.0019	42.3
813	P03995	Glial fibrillary acidic protein isoform 1	1.98	0.00072	26.7
939	P03995	Glial fibrillary acidic protein	1.13	0.004	29.3
935	–	–	1.47	0.01	–
924	Q8JJB8	Actin	1.12	0.011	47.5
985	–	–	1.16	0.034	–
998	P05063	Fructose-bisphosphate aldolase C OS	1.1	0.03	37.7
1029	Q9D154	Leukocyte elastase inhibitor A	−1.26	0.015	32.5
1045	Q9D6R2	Isocitrate dehydrogenase 3 (NAD^+) alpha	−1.12	0.0062	29.5
1156	P28663	Bete-soluble NSF attachment protein	−1.1	0.037	46.3
1195	P97429	Annexin A4	1.15	0.0093	3.4
1197	P08226	Apololoprotein E	1.53	0.0027	23.2
1259	Q9CPV4	Glyoxalase domain-containing protein 4	1.14	0.012	29.5
1274	P70202	Latexin	1.51	0.0021	29.3
1257	Q9CR00	26s proteasome non-ATPase regulatory subunit 9 OS	1.19	0.0031	18
1320	Q9R0P9	Ubiquitin carboxyl-terminal hydrolase isozyme L1	−1.16	0.0017	67.3
1340	–	–	1.6	0.002	–
1342	O08709	Peroxiredoxin-6	1.63	0.0016	63.8
1339	P14602	Heat shock protein 27	1.52	0.007	43.5
1395	Q9DCX2	ATP synthase subunit, mitochondrial	−1.19	0.0065	72.1
1367	P20108	Thioredoxin-dependent peroxide reductase, mitochondrial	−1.12	0.012	31.1
1469	P54227	Stathmin	−1.14	0.015	41.6
1533	Q05816	Fatty acid-binding protein	1.26	0.021	42.2

[a] p values determined in Student's t-test.
[b] Sequence coverage achieved by PMF.

Figs. 4I–L shows double immunofluorescence histochemistry for Prdx6 and GFAP in the anterior horn. In P301S tau-Tg mouse (Figs. 3I–L), immunoreactivity for Prdx6 was obviously present in GFAP-immuoreactive astrocytes, but not in the neurons (arrow in Fig. 4K indicates absence of neuronal staining) in the anterior horn. In Wt mouse (Fig. 4L), both immunoreactivity for Prdx6 and GFAP were rarely observed. Figs. 4M–P shows double immunofluorescence histochemistry for Prdx6 and GFAP in the white matter adjacent to the anterior horn. In P301S tau Tg mouse (Figs. 4M–O), immunoreactivity for Prdx6 was obviously present in GFAP-immuoreactive perikarya and their processes of astrocytes. In Wt mouse (Fig. 4P), Prdx6 was similarly colocalized with GFAP-immunoreactive perikarya and their processes of astrocytes.

Figs. 5A–D shows double immunofluorescence histochemistry for ApoE and GFAP in the anterior horn. In P301S tau-Tg mouse (Figs. 5A–C), ApoE was expressed in the both astrocytes and neurons (Fig. 5C; the arrow indicates a neuron, and the arrowhead indicates an astrocyte). In Wt mouse (Fig. 5D), ApoE was weakly positive in the neurons of the anterior horn. Figs. 5E–H shows double immunofluorescence histochemistry for ApoE and GFAP in the white matter adjacent to the anterior horn. In P301S tau-Tg mouse (Figs. 5E–G), immunoreactivity for ApoE was present in GFAP-immuoreactive perikarya and

Fig. 1 – Image of two-dimensional differential in-gel electrophoresis (2D-DIGE) between P301S human tau-Tg and Wt mouse. Spin protein extracts from P301S tau-Tg and Wt mouse were compared using the 2D-DIGE technique. A representative picture with spot numbers is shown in Fig. 1A. Representative four spots with upregulation were shown in Figs. 1B–E (spot number 1,197: ApoE, spot number 1,274: LTXN, spot number 1,339: Hsp27, spot number 1,342: Prdx6). Each of the left pictures depicted a merged picture of fluorescent dyes Cy3 and Cy5 (protein extracts from P301S tau-Tg were labeled by Cy3 as green fluorescence; those from Wt mouse were labeled by Cy5 as red fluorescence). Each of the right pictures depicted a merged picture of converse labeling (protein extracts from P301S tau-Tg were labeled by Cy5 as red fluorescence; those from Wt mouse were labeled by Cy3 as green fluorescence).

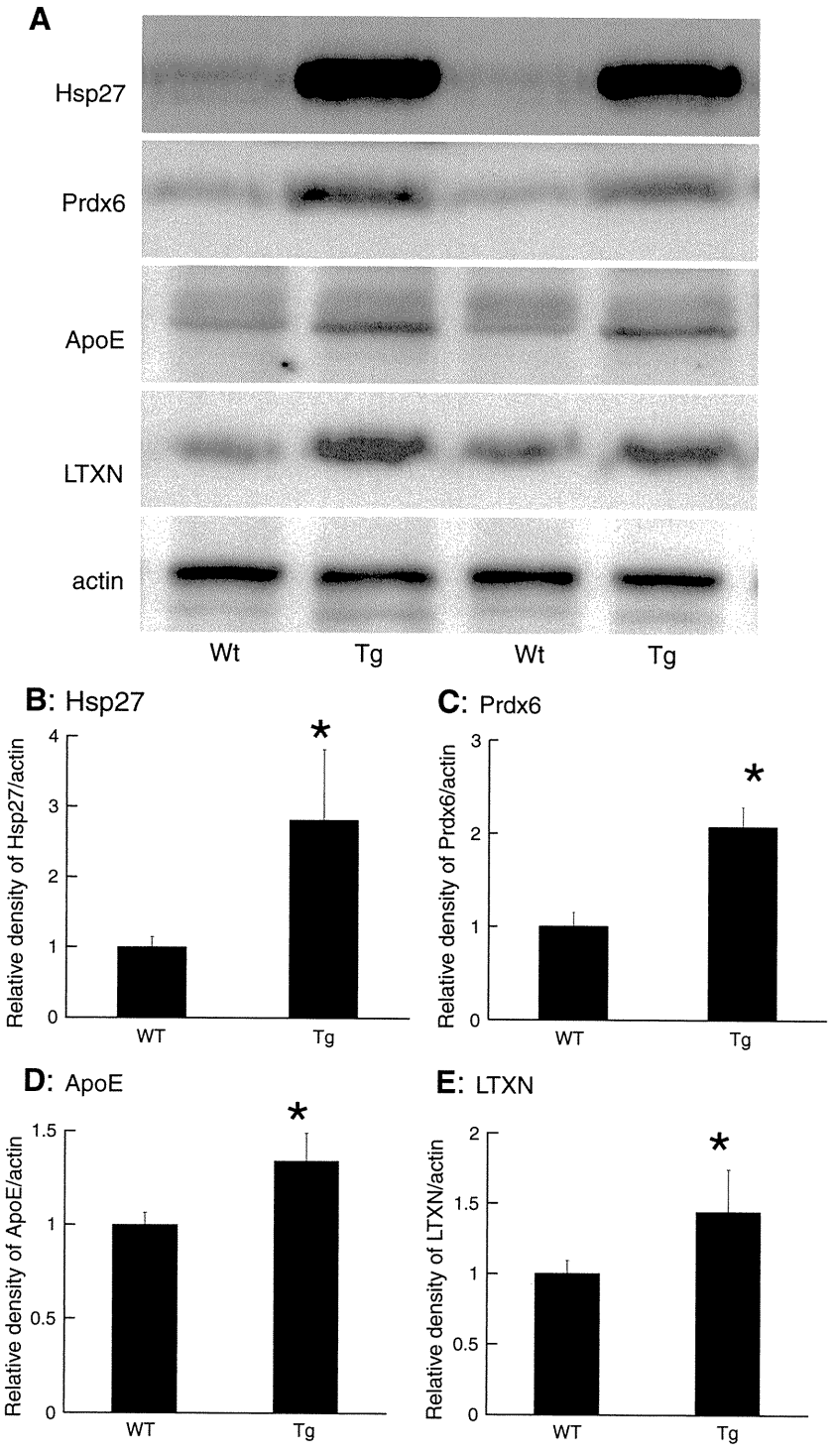

Fig. 2 – Western blotting of Hsp27, Prdx6, ApoE, and LTXN in Wt and P301S tau-Tg mouse. Western blotting was shown for Wt and P301S tau-Tg mice in duplicate in Fig. 2A. Figs. 2B, C, D, E indicates results of densitometry for Hsp27, Prdx6, ApoE, and LTXN, respectively, in P301S tau-Tg and Wt mice. Values were calculated as a relative to β-actin expression, and are expressed as mean ± standard deviation (SD). The asterisk indicates statistically significant differences between P301S tau-Tg and Wt mice. $p < 0.05$.

their processes of astrocytes. In Wt mouse (Fig. 5H), ApoE was weakly positive in astrocytic perikarya.

Figs. 5I–L shows double immunofluorescence histochemistry for LTXN and GFAP in the anterior horn. In P301S tau-Tg mouse (Figs. 5I–K), immunoreactivity for LTXN was obviously present in GFAP-immuoreactive astrocytes in the anterior horn, but not in neurons (arrow in Fig. 3I indicates absence of neuronal staining). In Wt mouse (Fig. 5L), both LTXN and GFAP

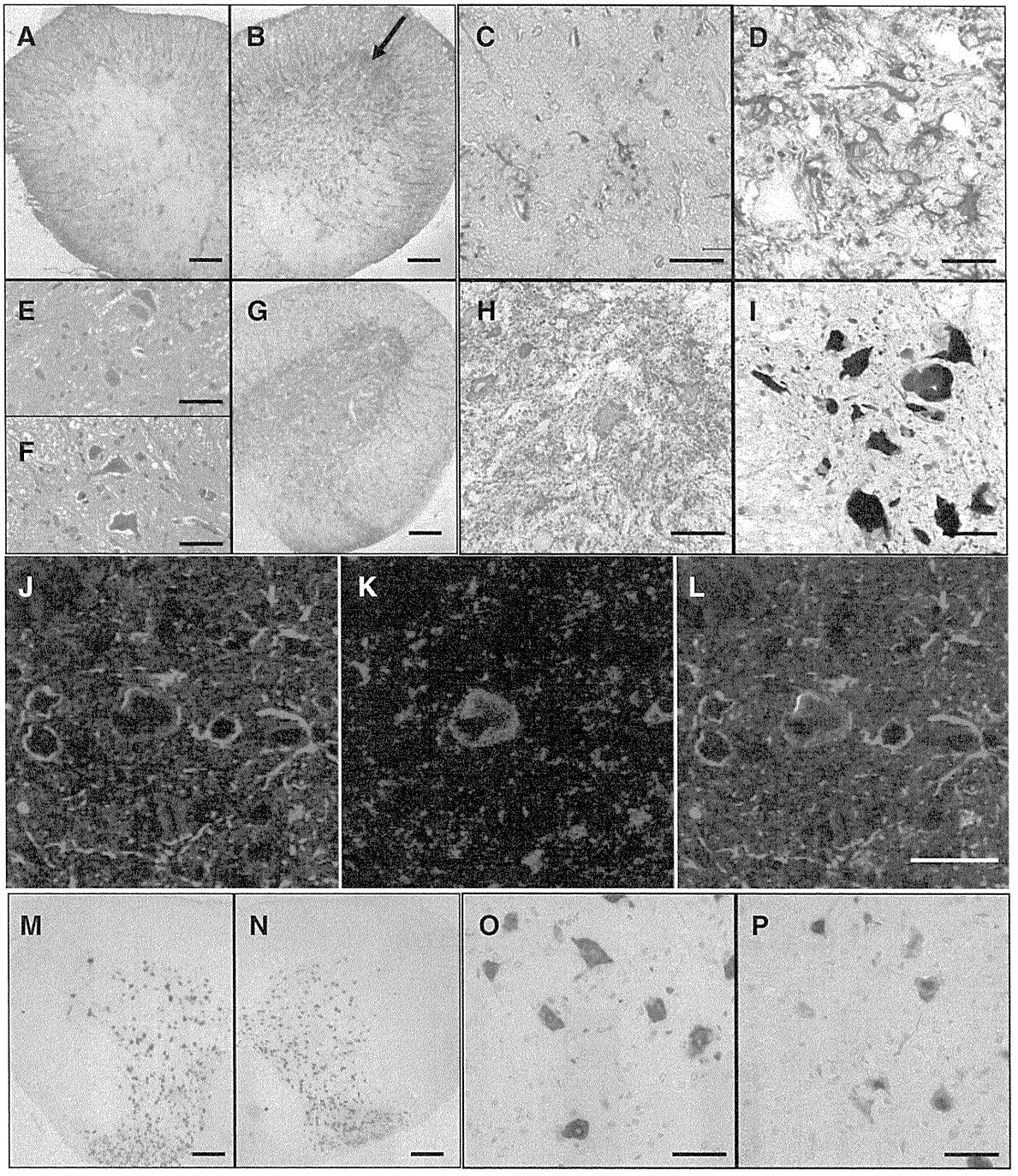

Fig. 3 – Photomicrographs of astrocytic infiltration and nerve cell loss in the sites of tau accumulation. Figs. 3A–D indicates immunostaining for GFAP in Wt (Figs. 3A, C) and P301S tau-Tg mouse (Figs. 3B, D). Figs. 3E and F is H&E staining in the anterior horn of Wt and P301S tau-Tg mouse, respectively. Figs. 3G and H shows immunohistochemistry for AT8, and Fig. 3I indicates Gallyas sliver staining in the anterior horn. Double immunofluorescence histochemistry was shown for GFAP (Fig. 3J) and AT8 (Fig. 3K) and their merge (Fig. 3L) in the anterior horn. Figs. 3M–P shows immunostaining for NeuN in the spinal cord in Wt (Figs. 3M, O) and P301S tau-Tg mouse (Figs. 3N, P). Scale bar: 20 μm in higher magnification, 100 μm in lower magnification.

were rarely stained. Figs. 5M–P shows double immunofluorescence histochemistry for LTXN and GFAP in the white matter adjacent to the anterior horn. In P301S tau-Tg mouse (Figs. 5M–O), immunoreactivity for LTXN was obviously colocalized with GFAP in the perikarya and their processes of astrocytes. In Wt mouse (Fig. 5P), LTXN was colocalized with GFAP-immunoreactive perikarya and their processes of astrocytes, similarly to P301S tau-Tg mouse.

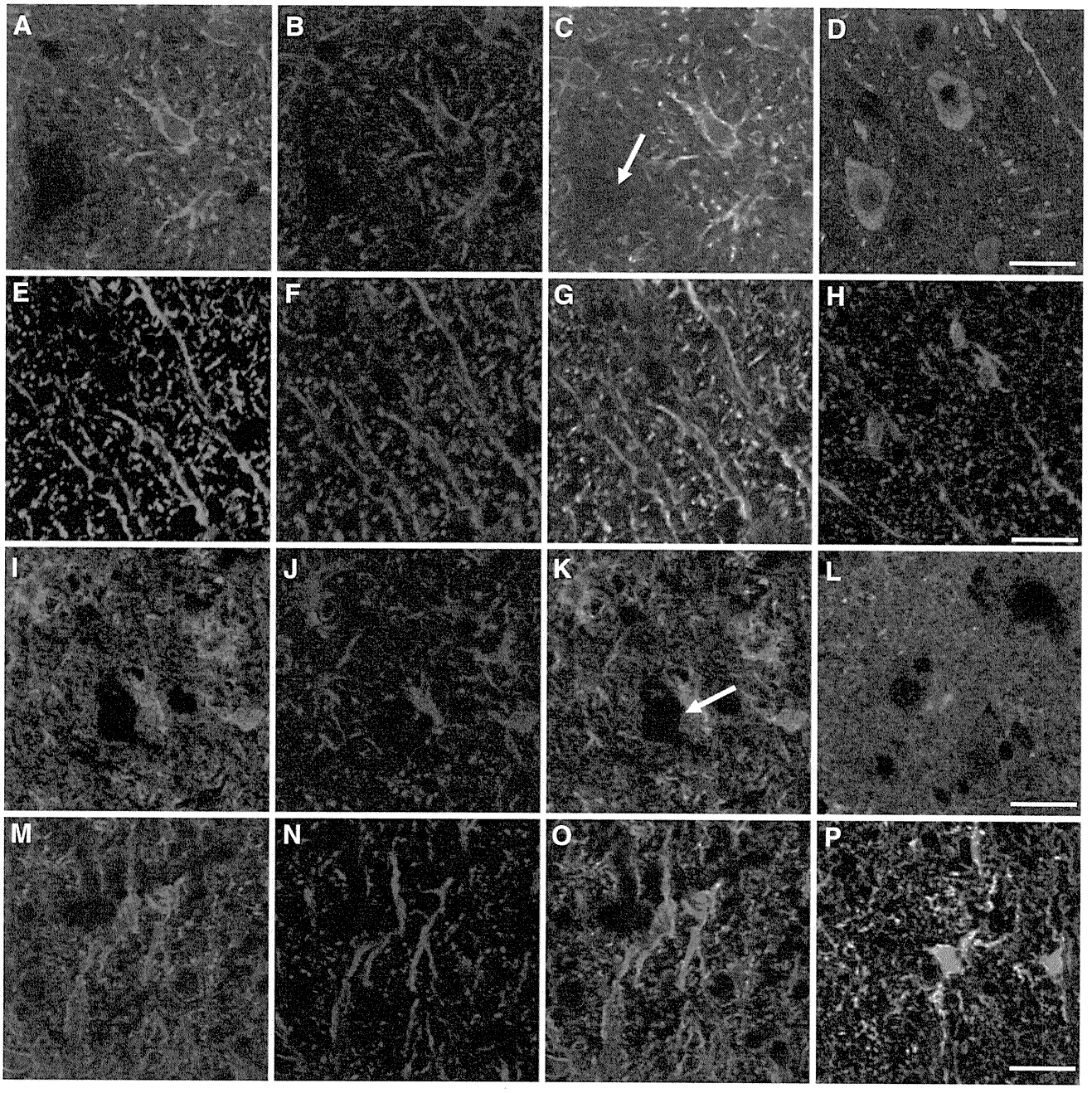

Fig. 4 – Photomicrographs of upregulated Hsp27 and Prdx6 in activated astrocytes. Double immunofluorescence histochemistry was shown for Hsp27 (Figs. 4A, E) and GFAP (Figs. 4B, F), and their merge in P301S tau-Tg mouse (Figs. 4C, G) and those in Wt mouse (Figs. 4D, H); for Prdx6 (Figs. 4I, M) and GFAP (Figs. 4J, N) and their merge in P301S tau-Tg mouse (Figs. 4K, O) and those in Wt mouse (Figs. 4L, P). The tissue sections were obtained from the anterior horn of the spinal cord (Figs. 4A–D, I–L) and the white matter (Figs. 4E–H, M–P). Scale bar: 20 μm.

3. Discussion

3.1. *Neuronal loss and astrocytic activation in tauopathy*

Tau protein in a hyperphosphorylated condition constitutes intracellular inclusions in neurodegenerative diseases. P301S tau-Tg mouse expressing human mutant tau exhibit essential features of tauopathies, including neurodegeneration and filamentous accumulation made of hyperphosphorylated tau protein. Proteomic analyses of the spinal cord of P301S human tau-Tg mouse identified upregulation of GFAP and four other proteins (Hsp27, Prdx6, ApoE, and LTXN). With immunohistochemistry, an increase of GFAP-immunoreactive astrocytes and neuronal loss were revealed in the anterior horn of the spinal cord which was one of the main sites of phosphorylated tau accumulation. These astrocytes also upregulated these four proteins; Hsp27, Prdx6, ApoE, and LTXN, which may have neuroprotective role against tau toxicity.

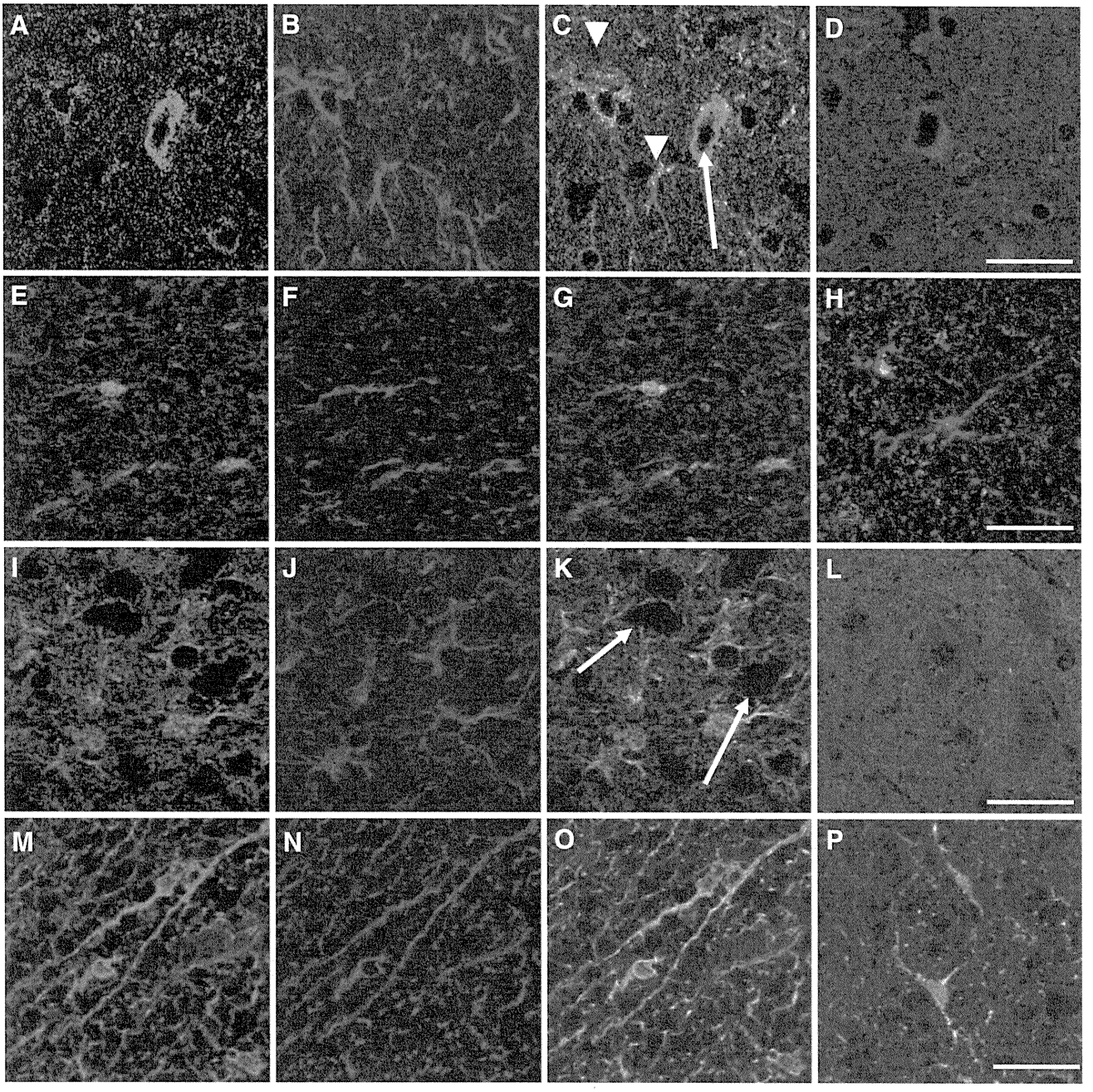

Fig. 5 – Photomicrographs of ApoE and LTXN upregulated in activated astrocytes. Double immunofluorescence histochemistry was shown for ApoE (Figs. 5A, E) and GFAP (Figs. 5B, F) and their merge in P301S tau-Tg mouse (Figs. 5C, G) and those in Wt mouse (Figs. 5D, H); for LTXN (Figs. 5I, M) and GFAP (Figs. 5J, N) and their merge in P301S tau-Tg mouse (Figs. 5K, O) and those in Wt mouse (Figs. 5L, P). The tissue sections were obtained from the anterior horn of the spinal cord (Figs. 5A–D, I–L) and the white matter (Figs. 5E–H, M–P). Scale bar: 20 μm.

Previously, it has been believed that endogenous, reactive astrocytes have a deleterious effect on the progression of FTD (Broe et al., 2004; Kersaitis et al., 2004; Tan et al., 2005). However, a recent study revealed that implantation of neural precursor cells into the brain resulted in glial cell differentiation, and amelioration of neuronal loss (Hampton et al., 2010). Taken together, the present study may indicate that astrocyte plays a beneficial role against neurodegeneration in conjunction with tau accumulation.

3.2. *Four proteins, which we identified in this study, may have protective role against tau toxicity*

Hsp27 is highly conserved and acts as molecular chaperones and/or have anti-apoptotic activities under physiological conditions (Franklin et al., 2005; Haslbeck, 2002). Expression of Hsp27 in the brain is notable because it is highly inducible in astrocytes and neurons following a wide range of noxious stimuli including cerebral ischemia (Plumier et al., 1997) and

epileptic seizure (Plumier et al., 1996). Moreover, induction of Hsp27 prevents neuronal cell death in noxious stimuli including ischemia (Wagstaff et al., 1999), peripheral nerve trans-section (Benn et al., 2002), and polyglutamine repeat expansion of huntingtin (Wyttenbach et al., 2002). On the protective mechanism of Hsp27 against tau toxicity, it is reported that Hsp27 directly combines with hyperphosphorylated tau in AD brains and can rescue cell death (Kosik and Shimura, 2005; Shimura et al., 2004b), while there are no reports of a direct relationship between Hsp27 and FTD. Interestingly, the amount of hyperphosphorylated tau is reduced with an increase of dephosphorylated tau, when Hsp27 is delivered with hyperphosphorylated tau, and this reduction is canceled by Hsp27 inhibitor (Shimura et al., 2004a). Therefore, they suggest that Hsp27 may facilitate degradation and/or dephosphorylation of pathological hyperphosphorylated tau in the AD brain.

Prdx6, also known as 1-Cys peroxiredoxin or non-selenium glutathione peroxidase, is a human brain antioxidant enzyme. Recent studies highlight involvement of oxidative stress in the etiology of tauopathies (Martínez et al., 2010; Melov et al., 2007), and show an interplay of tau phosphorylation and oxidative stress in the pathogenesis of neurofibrillary tangles (Takeda et al., 2000; Vanhelmont et al., 2010). Moreover, it is reported that astrocytes were the main target of oxidative stress in FTD (Martínez et al., 2008), although there are no studies on the relationship between Prdx6 and FTD. However, some studies indicate that Prdx6 is markedly enhanced in astrocytes in AD (Power et al., 2008), Parkinson's disease (Power et al., 2002) and Pick's disease (Krapfenbauer et al., 2003).

ApoE is a main lipoprotein present in the brain and is involved in the transport of plasma lipids, but its role in lipid and cholesterol homeostasis in the central nervous system remains unclear (Tomimoto et al., 1995). The ε4 allele of ApoE is a major genetic risk factor for AD. The relationship between ApoE and tau has not been thoroughly investigated and the results are much less clear than the relationship between ApoE and amyloid plaque burden (Kim et al., 2009). The important questions still exist as to whether it is better to increase or decrease ApoE levels in order to reduce neurofibrillary tangles. Under *in vitro* conditions, ApoE binds tightly to tau (Strittmatter et al., 1994) and has a protective role against neurotoxicity (Bruinsma et al., 2010). *In vivo*, lack of ApoE expression in mice resulted in an increase of neuroinflammation, thereby indicating anti-inflammatory effects of ApoE (Lynch et al., 2001; LaDu et al., 2001).

LTXN has been identified as a marker for neurons in the lateral neocortex of the developing mammalian brain. LTXN is the sole carboxypeptidase inhibitor (CPI) in the mammals, however, the cellular and molecular functions of LTXN in the central nervous system remain unclear (Liang and Van Zant, 2008). LTXN appears to play a role in the immune response *in vivo*, since latexin gene is highly expressed in macrophages and its expression is modulated by several proinflammatory stimuli (Aagaard et al., 2005). LTXN shows no significant homology with the other reported CPIs, but it shares a similar structure with a cystein protease inhibitor, cystatin C. Using an AD mouse model, two studies have shown that overexpression of cystatin C decreases amyloid-β, and thus may play a protective role in AD (Kaeser et al., 2007; Mi et al., 2007). In consideration of structural similarity between LTXN and cystatin C, LTXN expression in activated astrocytes in the present study may suggest a pivotal role for LTXN against tau toxicity.

In conclusion, we revealed astrocytic infiltration and neuronal loss in the lesions with hyperphosphorylated tau accumulation in P301S tauopathy model. These astrocytes preferentially upregulated four proteins presumed to have neuroprotective functions. Our data indicate significance of astrocytes which appear to be neuroprotective in tauopathy. In addition, the molecular mechanism of neuroprotection by astrocytes may provide a clue for a new strategy of astrocyte-based neuroprotective therapy in neurodegenerative disorders.

4. Experimental procedures

4.1. *Animals*

All experimental procedures were performed in strict adherence with the guidelines of the Animal Care and Ethics Committee of Mie University and the NIH Guide for the Care and Use of Laboratory Animals. P301S tau-Tg mice were kindly provided by Dr. Virginia M-Y Lee (The Center for Neurodegenerative Disease Research, Department of Pathology and Laboratory Medicine, University of Pennsylvania School of Medicine, Philadelphia, USA). P301S tau-Tg and Wt mice were bred in air-conditioned cages and were allowed free daily access to food and water.

4.2. *Sample preparation*

Mice at 7 months of age were deeply anesthetized and transcardially perfused with 15 ml of phosphate-buffered saline (PBS), and the spinal cord was removed (n=9 for P301S tau-Tg mice and Wt mice, respectively). The spinal cord was divided into two parts at the mid-thoracic level. The cervical–thoracic spinal cord was used for histology and immunohistochemistry and the thoracic–lumbar spinal cord was used for 2D-DIGE analysis and western blotting. The thoracic–lumbar spinal cord was immediately put into liquid nitrogen and stored at −80 °C until used. Frozen tissue (20–30 mg) was homogenized in lysis buffer (30 mM Tris–HCl, 7 M urea, 2 M thiourea, 4% w/v CHAPS, a protease inhibitor cocktail, pH 8.5). After incubation for 60 min on ice, homogenates were centrifuged at 30,000×*g* for 30 min at 4 °C and the supernatant was collected. Protein concentration of the supernatant was determined by the Bradford assay (Pierce, Rockford, IL) using bovine serum albumin as a standard. The cervical–thoracic spinal cord was fixed in 4% paraformaldehyde for 24 h with 10% formalin in PBS and embedded in paraffin.

4.3. *Two-dimensional difference in-gel electrophoresis (2D-DIGE)*

Each of 50 μg of protein from P301S tau-Tg mice (n=4) and Wt mice (n=4) was labeled with 200 pmol CyDye Fluor minimal dyes (GE Healthcare) of either Cy3, Cy5 as described in the manufacturer's protocols. Internal pools were generated by combining equal amounts of all samples and were labeled

with Cy2. Equal protein amounts of Cy2, Cy3, and Cy5-labeled samples were prepared. Protein extracts from P301S tau-Tg mouse were labeled by Cy3 and those from Wt mouse were labeled by Cy5 in two gels. Conversely, protein extracts from P301S tau-Tg mouse were labeled by Cy5 and those from Wt mouse were labeled by Cy3 in other two gels. These proteins were added to an equal volume of 2× sample buffer (7 M urea, 2 M thiourea, 4% w/v CHAPS, 130 mM dithiothreitol (DTT), 2% IPG buffer (pH 3–11, GE Healthcare), a protease inhibitor cocktail). After incubation on ice for 10 min in the dark, the samples were added to rehydration buffer (7 M urea, 2 M thiourea, 4% w/v CHAPS, 13 mM DTT, 1% IPG buffer (pI 3–11)) and a trace of bromophenol blue to make 450 μl of total sample volume. In-gel rehydration of the IPG strips (Immobiline Drystrips, 24 cm, pI 3–11, GE Healthcare) with the samples was performed overnight at room temperature. The first-dimension isoelectric focusing was run using an Ettan IPGphor (GE Healthcare) sequentially at 500 V for 500 Vh, at 1 kV for 1 kVh and at 8 kV for 99 kVh. After reduction and alkylation of disulfide bonds with 10 mg/ml DTT and 25 mg/ml iodoacetamide, respectively, the second-dimension 12.5% SDS-polyacrylamide gel electrophoresis (SDS-PAGE) was run on an Ettan DALT six Large Electrophoresis System (GE Healthcare).

4.4. *Imaging and analysis*

Gel images for analysis were obtained using a Typhoon 9400 imager (GE healthcare). The spots on the gel were co-detected automatically as Cy2, Cy3, Cy5 gel images. The resulting images were processed using DeCyder Differential Analysis Software (GE healthcare), which was designed specifically for 2D-DIGE experiments. Intra-gel matching was performed using the Cy2 internal standard images from each gel and the spot volume ratios of the Cy3- and Cy5-labeled spots were normalized with reference to the Cy2-labeled internal standard images. A Student's t-test was performed for every matched and normalized spot set, comparing the average and standard deviation of protein abundance for a given spot between the P301S tau-Tg and Wt mice. The protein spots were filtered to include only proteins that demonstrated a significant change ($p<0.05$) in abundance.

4.5. *Mass spectrometry*

For MS fingerprinting, the Coomassie Brilliant Blue-stained portions of the 2-D gel were excised and digested, as described previously (Kondo and Hirohashi, 2006) with the modifications. The differential protein spots on the gel were cut out, decolorized twice, dehydrated twice, added to 12.5 ng/ml trypsin (Promega) solution, and digested overnight at 37 °C. After each peptide segment was extracted, these samples were dried to 1–2 μl using speed vac. Then, each sample was mixed with 0.5 μl of saturated α-cyanohydroxycinnamic acid (CHCA) in 0.1% trifluoroacetic acid (TFA) and 45% acetonitrile, and dripped onto a stainless-steel target. MALDI-TOF/TOF mass spectrometry was performed using a 4800 Plus analyzer spectrometer (Applied Biosystems, Framingham, MA). Protein database searching was performed with the Paragon Method using Protein Pilot software (Applied Biosystems, Carlsbad, CA) to identify excised proteins. The following parameters were set for searching peptides using database: Uniplot; allow one missed cleavage; enzyme, trypsin; fixed modification, cysteine carbamidomethylation; variable modification, methionine oxidation.

4.6. *Western blotting*

Western blot analysis followed a standard protocol as described previously (Yata et al., 2007) (n=5 for P301S tau-Tg mice and Wt mice, respectively). Briefly, 6 μg of protein was loaded into each lane of precast polyacrylamide gel (ATTO corporation, Tokyo, Japan), and proteins were transferred onto PVDF membranes (Millipore, MA). The membranes were blocked with non-fat milk and then incubated with the primary antibodies which included rabbit polyclonal anti-POR6 (Abcam, Cambridge, MA, 1:1500), rabbit polyclonal anti-Hsp27 antibody (Abcam, Cambridge, MA, 1:1500), rabbit anti-ApoE antibody (Bioworld Technology, Inc., Louis Park, MN, 1:1000), and rabbit polyclonal anti-LTEX (ProteinTech Group, Inc., Chicago, IL, 1:1500). After incubation with appropriate horseradish peroxidase-conjugated secondary antibody (Santa Cruz Biotechnology, CA, 1:2,500) for 1 h at room temperature, immunoreactive bands were visualized in the linear range with the enhanced chemiluminescence ECL western blotting system (ECL Plus; Amersham Bioscience, Piscataway, NJ) and the CCD imager system (Image Quant Las 4000, GE Healthcare). After detection, membranes were stripped and reprobed with goat anti-actin antibody (Santa Cruz Biotechnology, Santa Cruz, CA). Quantitative evaluation of western blotting was performed using Multi Gauge Software (FUJIFILM, Tokyo, Japan), and values were calculated relative to expression level of β-actin as an appropriate compartment-specific intracellular protein. Results were expressed as mean±standard deviation (SD) and comparisons were made between P301S tau-Tg and Wt mice using Student's t-test, with $p<0.05$ considered statistically significant.

4.7. *Histology and immunohistochemistry*

Coronal spine sections (5 μm thickness) at the cervical level were prepared. Gallyas sliver staining and HE staining followed a standard protocol (Yoshiyama et al., 2007). Immunohistochemical analysis followed a standard protocol as described previously (Yata et al., 2007). The diaminobenzidine (DAB) staining method (ABC Staining Kit, Vector Laboratories, Inc., Burlingame, CA) was used for detection of GFAP, neuron specific nuclear protein (NeuN) and phosphorylation dependent tau included mouse monoclonal anti-phosphorylation dependent tau (AT8) (Innogenetics, Ghent, Belgium, 1:200), mouse monoclonal anti-GFAP (PROGEN Biotechnik, Heidelberg, Germany, 1:80), mouse monoclonal anti-neuron specific nuclear protein (NeuN) (Abcam. Cambridge, MA, 1:200). Immunofluorescence analysis followed a standard protocol as described previously (Yata et al., 2007), and included mouse monoclonal anti-phosphorylation dependent tau (AT8) (Innogenetics, Ghent, Belgium, 1:200), mouse monoclonal anti-GFAP (PROGEN Biotechnik, Heidelberg, Germany, 1:80), rabbit polyclonal anti-GFAP (Sigma, St. Louis, MO, 1:80), rabbit polyclonal anti-POR6 (Abcam. Cambridge, MA 1:100), rabbit polyclonal anti-Hsp27 antibody (Abcam. Cambride, MA 1:100), rabbit anti-ApoE antibody

(Bioworld Technology, Inc., Louis Park, MN 1:100), rabbit polyclonal anti-LTEX (Proteintech Group Inc., Chicago, IL, 1:100), and appropriate secondary antibodies, AlexaFluo 488 goat-anti rabbit IgG (Invitrogen, Carlsbad, CA, 1:250), AlexaFluo 594 goat-anti mouse IgG (Invitrogen, 1:250).

Acknowledgments

The authors have no personal, financial, or institutional interests in any of the drugs, materials, or devices described in this article. The authors appreciate Dr Virginia Lee for kindly providing the P301S tau-Tg mouse.

REFERENCES

Aagaard, A., Listwan, P., Cowieson, N., Huber, T., Ravasi, T., Wells, C.A., Flanagan, J.U., Kellie, S., Hume, D.A., Kobe, B., Martin, J.L., 2005. An inflammatory role for the mammalian carboxypeptidase inhibitor latexin: relationship to cystatins and the tumor suppressor TIG1. Structure 13, 309–317.

Allen, B., Ingram, E., Takao, M., Smith, M.J., Jakes, R., Virdee, K., Yoshida, H., Holzer, M., Craxton, M., Emson, P.C., Atzori, C., Migheli, A., Crowther, R.A., Ghetti, B., Spillantini, M.G., Goedert, M., 2002. Abundant tau filaments and nonapoptotic neurodegeneration in transgenic mice expressing human P301S tau protein. J. Neurosci. 22, 9340–9351.

Baba, Y., Baker, M.C., Le Ber, I., Brice, A., Maeck, L., Kohlhase, J., Yasuda, M., Stoppe, G., Bugiani, O., Sperfeld, A.D., Tsuboi, Y., Uitti, R.J., Farrer, M.J., Ghetti, B., Hutton, M.L., Wszolek, Z.K., 2007. Clinical and genetic features of families with frontotemporal dementia and parkinsonism linked to chromosome 17 with a P301S tau mutation. J. Neural Transm. 114, 947–950.

Bellucci, A., Westwood, A.J., Ingram, E., Casamenti, F., Goedert, M., Spillantini, M.G., 2004. Induction of inflammatory mediators and microglial activation in mice transgenic for mutant human P301S tau protein. Am. J. Pathol. 165, 1643–1652.

Benn, S.C., Perrelet, D., Kato, A.C., Scholz, J., Decosterd, I., Mannion, R.J., Bakowska, J.C., Woolf, C.J., 2002. Hsp27 upregulation and phosphorylation is required for injured sensory and motor neuron survival. Neuron 36, 45–56.

Broe, M., Kril, J., Halliday, G.M., 2004. Astrocytic degeneration relates to the severity of disease in frontotemporal dementia. Brain 127, 2214–2220.

Bruinsma, I.B., Wilhelmus, M.M., Kox, M., Veerhuis, R., de Waal, R.M., Verbeek, M.M., 2010. Apolipoprotein E protects cultured pericytes and astrocytes from D-Abeta(1–40)-mediated cell death. Brain Res. 1315, 169–180.

Delobel, P., Lavenir, I., Fraser, G., Ingram, E., Holzer, M., Ghetti, B., Spillantini, M.G., Crowther, R.A., Goedert, M., 2008. Analysis of tau phosphorylation and truncation in a mouse model of human tauopathy. Am. J. Pathol. 172, 123–131.

Franklin, T.B., Krueger-Naug, A.M., Clarke, D.B., Arrigo, A.P., Currie, R.W., 2005. The role of heat shock proteins Hsp70 and Hsp27 in cellular protection of the central nervous system. Int. J. Hyperthermia 21, 379–392.

Hampton, D.W., Webber, D.J., Bilican, B., Goedert, M., Spillantini, M.G., Chandran, S., 2010. Cell-mediated neuroprotection in a mouse model of human tauopathy. J. Neurosci. 30, 9973–9983.

Haslbeck, M., 2002. Hsps and their role in the chaperone network. Cell. Mol. Life Sci. 59, 1649–1657.

Iqbal, K., Liu, F., Gong, C.X., Alonso, Adel C., Grundke-Iqbal, I., 2009. Mechanisms of tau-induced neurodegeneration. Acta Neuropathol. 118, 53–69.

Kersaitis, C., Halliday, G.M., Kril, J.J., 2004. Regional and cellular pathology in frontotemporal dementia: relationship to stage of disease in cases with and without Pick bodies. Acta Neuropathol. 108, 515–523.

Kosik, K.S., Shimura, H., 2005. Phosphorylated tau and the neurodegenerative foldopathies. Biochim. Biophys. Acta 1739, 298–310.

LaDu, M.J., Shah, J.A., Reardon, C.A., Getz, G.S., Bu, G., Hu, J., Guo, L., Van Eldik, L.J., 2001. Apolipoprotein E and apolipoprotein E receptors modulate A beta-induced glial neuroinflammatory responses. Neurochem. Int. 39, 427–434.

Lee, V.M., Goedert, M., Trojanowski, J.Q., 2001. Neurodegenerative tauopathies. Annu. Rev. Neurosci. 24, 1121–1159.

Liang, Y., Van Zant, G., 2008. Aging stem cells, latexin, and longevity. Exp. Cell Res. 314, 1962–1972.

Lynch, J.R., Morgan, D., Mance, J., Matthew, W.D., Laskowitz, D.T., 2001. Apolipoprotein E modulates glial activation and the endogenous central nervous system inflammatory response. J. Neuroimmunol. 114, 107–113.

Kaeser, S.A., Herzig, M.C., Coomaraswamy, J., Kilger, E., Selenica, M.L., Winkler, D.T., Staufenbiel, M., Levy, E., Grubb, A., Jucker, M., 2007. Cystatin C modulates cerebral beta-amyloidosis. Nat. Genet. 39, 1437–1439.

Kim, J., Basak, J.M., Holtzman, D.M., 2009. The role of apolipoprotein E in Alzheimer's disease. Neuron 63, 287–303.

Kondo, T., Hirohashi, S., 2006. Application of highly sensitive fluorescent dyes (CyDye DIGE Fluor saturation dyes) to laser microdissection and two-dimensional difference gel electrophoresis (2D-DIGE) for cancer proteomics. Nat. Protoc. 1, 2940–2956.

Krapfenbauer, K., Engidawork, E., Cairns, N., Fountoulakis, M., Lubec, G., 2003. Aberrant expression of peroxiredoxin subtypes in neurodegenerative disorders. Brain Res. 967, 152–160.

Martínez, A., Carmona, M., Portero-Otin, M., Naudí, A., Pamplona, R., Ferrer, I., 2008. Type-dependent oxidative damage in frontotemporal lobar degeneration: cortical astrocytes are targets of oxidative damage. J. Neuropathol. Exp. Neurol. 67, 1122–1136.

Martínez, A., Portero-Otin, M., Pamplona, R., Ferrer, I., 2010. Protein targets of oxidative damage in human neurodegenerative diseases with abnormal protein aggregates. Brain Pathol. 20, 281–297.

Melov, S., Adlard, P.A., Morten, K., Johnson, F., Golden, T.R., Hinerfeld, D., Schilling, B., Mavros, C., Masters, C.L., Volitakis, I., Li, Q.X., Laughton, K., Hubbard, A., Cherny, R.A., Gibson, B., Bush, A.I., 2007. Mitochondrial oxidative stress causes hyperphosphorylation of tau. PLoS One 20, e536.

Mi, W., Pawlik, M., Sastre, M., Jung, S.S., Radvinsky, D.S., Klein, A.M., Sommer, J., Schmidt, S.D., Nixon, R.A., Mathews, P.M., Levy, E., 2007. Cystatin C inhibits amyloid-beta deposition in Alzheimer's disease mouse models. Nat. Genet. 39, 1440–1442.

Plumier, J.C., Armstrong, J.N., Landry, J., Babity, J.M., Robertson, H.A., Currie, R.W., 1996. Expression of the 27,000 mol. wt heat shock protein following kainic acid-induced status epilepticus in the rat. Neuroscience 75, 849–856.

Plumier, J.C., Armstrong, J.N., Wood, N.I., Babity, J.M., Hamilton, T.C., Hunter, A.J., Robertson, H.A., Currie, R.W., 1997. Differential expression of c-fos, Hsp70 and Hsp27 after photothrombotic injury in the rat brain. Mol. Brain Res. 45, 239–246.

Power, J.H., Shannon, J.M., Blumbergs, P.C., Gai, W.P., 2002. Nonselenium glutathione peroxidase in human brain: elevated levels in Parkinson's disease and dementia with lewy bodies. Am. J. Pathol. 161, 885–894.

Power, J.H., Asad, S., Chataway, T.K., Chegini, F., Manavis, J., Temlett, J.A., Jensen, P.H., Blumbergs, P.C., Gai, W.P., 2008. Peroxiredoxin 6 in human brain: molecular forms, cellular distribution and association with Alzheimer's disease pathology. Acta Neuropathol. 115, 611–622.

Shimura, H., Schwartz, D., Gygi, S.P., Kosik, K.S., 2004a. CHIP-Hsc70 complex ubiquitinates phosphorylated tau and enhances cell survival. J. Biol. Chem. 279, 4869–4876.

Shimura, H., Shimura, Y.M., Kosik, K.S., 2004b. Binding of tau to heat shock protein 27 leads to decreased concentration of hyperphosphorylated tau and enhanced cell survival. J. Biol. Chem. 279, 17957–17962.

Strittmatter, W.J., Saunders, A.M., Goedert, M., Weisgraber, K.H., Dong, L.M., Jakes, R., Huang, D.Y., Pericak-Vance, M., Schmechel, D., Roses, A.D., 1994. Isoform-specific interactions of apolipoprotein E with microtubule-associated protein tau: implications for Alzheimer disease. Proc. Natl. Acad. Sci. 91, 11183–11186.

Takeda, A., Smith, M.A., Avilá, J., Nunomura, A., Siedlak, S.L., Zhu, X., Perry, G., Sayre, L.M., 2000. In Alzheimer's disease, heme oxygenase is coincident with Alz50, an epitope of tau induced by 4-hydroxy-2-nonenal modification. J. Neurochem. 75, 1234–1241.

Tan, C.F., Piao, Y.S., Kakita, A., Yamada, M., Takano, H., Tanaka, M., Mano, A., Makino, K., Nishizawa, M., Wakabayashi, K., Takahashi, H., 2005. Frontotemporal dementia with co-occurrence of astrocytic plaques and tufted astrocytes, and severe degeneration of the cerebral white matter: a variant of corticobasal degeneration? Acta Neuropathol. 109, 329–338.

Tomimoto, H., Akiguchi, I., Suenaga, T., Wakita, H., Nakamura, S., Kimura, J., Budka, H., 1995. Immunohistochemical study of apolipoprotein E in human cerebrovascular white matter lesions. Acta Neuropathol. 90, 608–614.

Trojanowski, J.Q., Ishihara, T., Higuchi, M., Yoshiyama, Y., Hong, M., Zhang, B., Forman, M.S., Zhukareva, V., Lee, V.M., 2002. Amyotrophic lateral sclerosis/parkinsonism dementia complex: transgenic mice provide insights into mechanisms underlying a common tauopathy in an ethnic minority on Guam. Exp. Neurol. 176, 1–11.

Tsuboi, Y., 2006. Neuropathology of familial tauopathy Neuropathology 26, 471–474.

Vanhelmont, T., Vandebroek, T., De Vos, A., Terwel, D., Lemaire, K., Anandhakumar, J., Franssens, V., Swinnen, E., Van Leuven, F., Winderickx, J., 2010. Serine-409 phosphorylation and oxidative damage define aggregation of human protein tau in yeast. FEMS Yeast Res. 10, 992–1005.

Wagstaff, M.J., Collaço-Moraes, Y., Smith, J., de Belleroche, J.S., Coffin, R.S., Latchman, D.S., 1999. Protection of neuronal cells from apoptosis by Hsp27 delivered with a herpes simplex virus-based vector. J. Biol. Chem. 274, 5061–5069.

Wyttenbach, A., Sauvageot, O., Carmichael, J., Diaz-Latoud, C., Arrigo, A.P., Rubinsztein, D.C., 2002. Heat shock protein 27 prevents cellular polyglutamine toxicity and suppresses the increase of reactive oxygen species caused by huntingtin. Hum. Mol. Genet. 11, 1137–1151.

Yata, K., Matchett, G.A., Tsubokawa, T., Tang, J., Kanamaru, K., Zhang, J.H., 2007. Granulocyte-colony stimulating factor inhibits apoptotic neuron loss after neonatal hypoxia–ischemia in rats. Brain Res. 1145, 227–238.

Yoshiyama, Y., Higuchi, M., Zhang, B., Huang, S.M., Iwata, N., Saido, T.C., Maeda, J., Suhara, T., Trojanowski, J.Q., Lee, V.M., 2007. Synapse loss and microglial activation precede tangles in a P301S tauopathy mouse model. Neuron 53, 337–351.

Journal of Human Genetics (2011) 56, 401–403

www.nature.com/jhg

SHORT COMMUNICATION

PLA2G6 variant in Parkinson's disease

Hiroyuki Tomiyama[1,5], Hiroyo Yoshino[2,5], Kotaro Ogaki[1], Lin Li[1], Chikara Yamashita[1], Yuanzhe Li[2], Manabu Funayama[1,2], Ryogen Sasaki[3], Yasumasa Kokubo[3], Shigeki Kuzuhara[4] and Nobutaka Hattori[1,2]

PLA2G6 **was reported recently as the causative gene for *PARK14*-linked autosomal recessive early-onset dystonia-parkinsonism. In a recent study in Singapore, heterozygous *PLA2G6* p.P806R (c.2417C>G) mutation in exon 17 was reported to be a possible Parkinson's disease (PD)-related mutation. To determine the significance of the *PLA2G6* mutation, we conducted an association study by performing direct sequencing of *PLA2G6* exon 17 in 379 Japanese sporadic PD patients and 310 controls in the Japanese general population. In this group, we found 12 patients (12/379=3.16%) and 10 controls (10/310=3.23%) with a heterozygous p.P806R mutation (P=0.96, χ^2=0.0019). Therefore, our large case–controlled study suggests that *PLA2G6* p.P806R is not a disease-associated polymorphism in PD. Moreover, we performed direct sequencing of all exons and exon-intron boundaries of *PLA2G6* in 116 Japanese patients with sporadic PD. Two single heterozygous variants (p.R301C or p.D331N) were found (both frequencies: 1/379 patients vs 0/310 controls) and the roles of their variants were unclear. Finally, combined with the previous report, our findings emphasize that *PLA2G6* mutations are unlikely to be the major causes or risk factors of PD at least in Asian populations. However, further large studies in various populations are needed because patients with *PLA2G6* mutations can show heterogeneous clinical features.**
Journal of Human Genetics (2011) **56,** 401–403; doi:10.1038/jhg.2011.22; published online 3 March 2011

Keywords: genetics; Parkinson's disease; parkinsonism-dystonia; *PLA2G6*; *PARK14*

Parkinson's disease (PD, OMIM no. 168600) is the second most common neurodegenerative disorder next to Alzheimer's disease. Although the cause remains unclear, PD is thought to be a heterogeneous disease caused by the interaction of multiple genetic factors and environmental factors associated with aging. Indeed, case–control studies identified some genetic risk factors for PD, such as *SNCA*,[1–4] *LRRK2*[3–8] and *GBA* variants.[9–11] To elucidate the exact etiology of PD, identifying the effect of each of the multiple factors and their combined effects is important.

Recently, *PLA2G6* was reported to be the causative gene for *PARK14* in patients with autosomal recessive early-onset dystonia-parkinsonism.[12] *PLA2G6* is also the causative gene for infantile neuroaxonal dystrophy, neurodegeneration associated with brain iron accumulation and Karak syndrome.[13–15] Some patients with neurodegeneration associated with brain iron accumulation show very early-onset and rapid psychomotor regression, early cerebellar signs, pyramidal signs and visual disturbances. Patients with *PLA2G6* mutations frequently exhibit brain iron accumulation, which is a feature of neurodegeneration associated with brain iron accumulation. In our recent study, we revealed two novel compound heterozygous *PLA2G6* mutations in Japanese patients who had levodopa-responsive parkinsonism with or without brain iron accumulation.[16] Although there are few *PLA2G6* mutation analyses in parkinsonism so far, its role in parkinsonism or PD and the mechanism of neurodegeneration and iron accumulation have not been clarified.

Very recently, Tan *et al.*[17] in Singapore reported the results of *PLA2G6* analysis in 96 PD patients with young-age onset/dystonia. One of the 96 patients, who had a novel heterozygous p.P806R (c.2417C>G) mutation in exon 17, had typical features of late-onset PD with levodopa responsiveness and dystonic spasms. Although they could not conduct a segregation analysis, this mutation was not found in 100 healthy controls. Their result emphasized the potential role of this mutation and the *PLA2G6* mutation as pathogenic mutations or risk factors for PD in Chinese or other races. To confirm this intriguing finding of *PLA2G6*, we conducted an extended mutation analysis and association study in Japanese patients with sporadic PD and normal controls.

The study was approved by the Institutional Review Board of Juntendo University, and all subjects provided an informed consent. We collected blood samples from each participant and extracted genomic DNA by using standard methods. Sequences of the primers/probes and conditions of PCR/sequencing are available upon request to the corresponding author or the first author. We directly sequenced the exon 17 of *PLA2G6* from 379 Japanese patients with sporadic PD and 310 normal Japanese subjects as controls (Table 1).

[1]Department of Neurology, Juntendo University School of Medicine, Tokyo, Japan; [2]Research Institute for Diseases of Old Age, Graduate School of Medicine, Juntendo University, Tokyo, Japan; [3]Department of Neurology, Mie University School of Medicine, Mie, Japan and [4]Department of Medical Welfare, the Faculty of Health Science, Suzuka University of Medical Science, Mie, Japan
[5]These authors contributed equally to this work.
Correspondence: Professor N Hattori, Department of Neurology, Juntendo University School of Medicine, 2-1-1 Hongo, Bunkyo-ku, Tokyo 113-8421, Japan.
E-mail: nhattori@juntendo.ac.jp
Received 17 July 2010; revised 18 January 2011; accepted 27 January 2011; published online 3 March 2011

Table 1 Profile of analyzed subjects and allele frequency of *PLA2G6* p.P806R (c.2417C>G) in Japanese patients with sporadic Parkinson's disease (SPD) and control subjects from the general population

	Japanese SPD			*Japanese control from the general population*		
	All analyzed subjects	*Heterozygous (C/G)*	*Wild type (C/C)*	*All analyzed subjects*	*Heterozygous (C/G)*	*Wild type (C/C)*
Number of patients (F:M)	379 (198:181)	12 (3:9)	367 (195:172)	310 (188:122)	10 (6:4)	300 (182:118)
Age at sampling[a] (range, *n*=number)	60.2 ± 14.0 (12–92, *n*=378)	58.6 ± 22.4 (12–87, *n*=12)	60.3 ± 13.7 (12–92, *n*=366)	58.5 ± 13.2 (23–98, *n*=294)	60.7 ± 12.8 (35–81, *n*=10)	58.5 ± 13.2 (23–98, *n*=284)
Age at onset[a] (range, *n*=number)	52.7 ± 14.3 (7–88, *n*=375)	52.7 ± 22.3 (11–83, *n*=12)	52.7 ± 14.0 (7–88, *n*=365)			
Disease duration[a] (range, *n*=number)	7.4 ± 5.6 (0–40, *n*=375)	5.9 ± 5.3 (1–18, *n*=12)	7.5 ± 5.6 (0–40, *n*=363)			
Allele frequency (%)		1.58			1.61	

No homozygous *PLA2G6* p.P806R mutation was found in this study. Genotypes of the patients and controls were concordant with Hardy–Weinberg equilibrium.
[a]Data are mean ± s.d.

We identified a heterozygous p.P806R mutation in 12 patients with PD and in 10 controls (χ^2=0.0019, P=0.96; odds ratio (genotype)=1.02, 95% confidence interval: 0.44–2.37, Table 1). We found no homozygous p.P806R mutations. The allele frequency was 1.58% in sporadic PD and 1.61% in controls. We also found heterozygous synonymous p.T787T (c.2355C>T) variant in two patients and one control. No other variants were found in exon 17. Moreover, we performed direct sequencing of all exons and exon–intron boundaries of *PLA2G6* in 116 Japanese patients with sporadic PD (males 60, females 56; age range, 12–92 years; mean age, 60.7 ± 18.1 years; mean disease duration, 6.3 ± 5.8 years). Among them, we found two novel single heterozygous non-synonymous variants (p.R301C, p.D331N). Both frequencies of the two variants were 1/379=0.26% in patients and 0/310=0% in Japanese normal controls. The roles of their rare variants found in Japanese patients with sporadic PD remained unclear (Table 2).

The reported clinical features of neurodegeneration associated with mutations in the *PLA2G6* gene (PLAN) are axonal dystrophy, dystonia, dementia, visual disturbances, cerebellar signs and brain atrophy with or without iron accumulation.[12–15,18,19] Showing clinical heterogeneity, patients with *PARK14*-linked parkinsonism have levodopa responsiveness, levodopa-induced dyskinesia and dementia with an older-age onset and a longer disease duration than those with infantile neuroaxonal dystrophy.[12,16] These studies have suggested that patients with *PLA2G6* mutation can show heterogeneous phenotype.

Although the precise function of *PLA2G6* in neurodegeneration and iron accumulation remains obscure, defective phospholipid metabolism is implicated in neurodegenerative diseases featuring brain iron dyshomeostasis.[14] *PLA2G6* is thought to be responsible for the development of autosomal recessive disorders through its loss of function; hence, the role of a single heterozygous *PLA2G6* mutation is intriguing. Indeed, two of the 10 infantile neuroaxonal dystrophy patients were previously reported to have one-allele mutations, suggesting that single heterozygous mutation in *PLA2G6* could be pathogenic.[19]

The aim of this study was to clarify the role of the *PLA2G6* mutation in PD. Although patients with *PLA2G6* mutations have been reported to show atypical parkinsonism, the heterozygous *PLA2G6* p.P806R mutation was found in late-onset PD patients with typical parkinsonism.[17] In our extended case–controlled study of a large sample size, no association of *PLA2G6* p.P806R was identified in Japanese PD patients and controls. Thus, our data suggest that *PLA2G6* p.P806R is a non-PD-associated polymorphism at least in Japanese PD patients. This result should help clinicians in genetic counseling for PD patients.

Furthermore, in the previous report, there were no other possible PD-associated variants in any of the 17 exons in the 96 PD patients.[17] Therefore, combined with the data from Singapore,[17] our findings emphasize that *PLA2G6* mutations are unlikely to be the major causes or risk factors of PD at least in Asian populations.

However, because there have been no adequate *PLA2G6* mutation analyses in parkinsonism, disease-associated variants in *PLA2G6* could exist in patients with atypical/typical parkinsonism, or PD in specific races. In parkinsonism-dystonia patients, *PLA2G6* mutations have thus far been reported in only certain populations, such as Indians, Pakistanis and Iranians.[12,15,19] In heterogeneous clinical setting of patients with *PLA2G6* mutations, the roles of *PLA2G6* should be clarified including the effect of heterozygous mutation. As brain iron accumulation is frequently observed in common diseases, such as PD and Alzheimer's disease, the role of *PLA2G6* in iron accumulation is elusive in neurodegenerative disorders.

Table 2 *PLA2G6* variants (excluding p.P806R) found in patients with sporadic PD and the allele frequency

				Frequency in this study		
Exon	*Position*	*Amino acid*	*Accession number*	*Patients (%)*	*Allele frequency in patients (%)*	*Controls (%)*
2	c.87G>A	p.V29V	rs2267369	18/116 (15.52)	8.19	
7	c.901C>T	p.R301C	(novel)	1/379 (0.26)	0.13	0/310 (0)
7	c.991G>A	p.D331N	(novel)	1/379 (0.26)	0.13	0/310 (0)

Abbreviation: PD, Parkinson's disease.

Thus, further large studies in various populations and functional studies for *PLA2G6* are needed in neurodegenerative disorders with or without brain iron accumulation.

CONFLICT OF INTEREST

The authors declare no conflict of interest.

ACKNOWLEDGEMENTS

We thank all participants. This study was supported by a grant from the Japanese Ministry of Education, Culture, Sports, Science and Technology, Grants-in-Aid for Scientific Research (to HT: 21591098 and to NH: 09005213), for Scientific Research on Priority Areas (to NH: 08071510), and for Young Scientists (to MF: 22790829) and Health and Labour Sciences Research Grants from the Japanese Ministry of Health, Labour and Welfare (to NH: H19-021 and H20-015). This work was partially supported by Grants-in-Aid from the Research Committee of CNS Degenerative Diseases and Perry syndrome (to NH and HT: 22140901) and of CNS Degenerative Diseases and Muro disease (Kii ALS/PDC), the Ministry of Health, Labour and Welfare of Japan (to YK: 21210301).

1 Mueller, J. C., Fuchs, J., Hofer, A., Zimprich, A., Lichtner, P., Illig, T. *et al.* Multiple regions of alpha-synuclein are associated with Parkinson's disease. *Ann. Neurol.* **57,** 535–541 (2005).
2 Mizuta, I., Satake, W., Nakabayashi, Y., Ito, C., Suzuki, S., Momose, Y. *et al.* Multiple candidate gene analysis identifies alpha-synuclein as a susceptibility gene for sporadic Parkinson's disease. *Hum. Mol. Genet.* **15,** 1151–1158 (2006).
3 Satake, W., Nakabayashi, Y., Mizuta, I., Hirota, Y., Ito, C., Kubo, M. *et al.* Genome-wide association study identifies common variants at four loci as genetic risk factors for Parkinson's disease. *Nat. Genet.* **41,** 1303–1307 (2009).
4 Simón-Sánchez, J ., Schulte, C., Bras, J. M., Sharma, M., Gibbs, J. R., Berg, D. *et al.* Genome-wide association study reveals genetic risk underlying Parkinson's disease. *Nat. Genet.* **41,** 1308–1312 (2009).
5 Di Fonzo, A., Wu-Chou, Y. H., Lu, C. S., van Doeselaar, M., Simons, E. J., Rohé, C. F. *et al.* A common missense variant in the LRRK2 gene, Gly2385Arg, associated with Parkinson's disease risk in Taiwan. *Neurogenetics.* **7,** 133–138 (2006).
6 Tan, E. K., Zhao, Y., Skipper, L., Tan, M. G., Di Fonzo, A., Sun, L. *et al.* The *LRRK2* Gly2385Arg variant is associated with Parkinson's disease: genetic and functional evidence. *Hum. Genet.* **120,** 857–863 (2007).
7 Funayama, M., Li, Y., Tomiyama, H., Yoshino, H., Imamichi, Y., Yamamoto, M. *et al.* Leucine-rich repeat kinase 2 G2385R variant is a risk factor for Parkinson disease in Asian population. *Neuroreport.* **18,** 273–275 (2007).
8 Ross, O. A., Wu, Y. R., Lee, M. C., Funayama, M., Chen, M. L., Soto, A. I. *et al.* Analysis of Lrrk2 R1628P as a risk factor for Parkinson's disease. *Ann. Neurol.* **64,** 88–92 (2008).
9 Aharon-Peretz, J., Rosenbaum, H. & Gershoni-Baruch, R. Mutations in the glucocerebrosidase gene and Parkinson's disease in Ashkenazi Jews. *N. Engl. J. Med.* **351,** 1972–1977 (2004).
10 Mitsui, J., Mizuta, I., Toyoda, A., Ashida, R., Takahashi, Y., Goto, J. *et al.* Mutations for Gaucher disease confer high susceptibility to Parkinson disease. *Arch. Neurol.* **66,** 571–576 (2009).
11 Sidransky, E., Nalls, M. A., Aasly, J. O., Aharon-Peretz, J., Annesi, G., Barbosa, E. R. *et al.* Multicenter analysis of glucocerebrosidase mutations in Parkinson's disease. *N. Engl. J. Med.* **361,** 1651–1661 (2009).
12 Paisan-Ruiz, C., Bhatia, K. P., Li, A., Hernandez, D., Davis, M., Wood, N. W. *et al.* Characterization of PLA2G6 as a locus for dystonia-parkinsonism. *Ann. Neurol.* **65,** 19–23 (2009).
13 Aicardi, J. & Castelein, P. Infantile neuroaxonal dystrophy. *Brain.* **102,** 727–748 (1979).
14 Morgan, N. V., Westaway, S. K., Morton, J. E., Gregory, A., Gissen, P., Sonek, S. *et al.* PLA2G6 encoding a phospholipase A2, is mutated in neurodegenerative disorders with high brain iron. *Nat. Genet.* **38,** 752–754 (2006).
15 Mubaidin, A., Roberts, E., Hampshire, D., Dehyyat, M., Shurbaji, A., Mubaidien, M. *et al.* Karak syndrome: a novel degenerative disorder of the basal ganglia and cerebellum. *J. Med. Genet.* **40,** 543–546 (2003).
16 Yoshino, H., Tomiyama, H., Tachibana, N., Ogaki, K., Li, Y., Funayama, M. *et al.* Phenotypic spectrum of patients with PLA2G6 mutation and PARK14-linked parkinsonism. *Neurology.* **75,** 1356–1361 (2010).
17 Tan, E. K., Ho, P., Tan, L., Prakash, K. M. & Zhao, Y. PLA2G6 mutations and Parkinson's disease. *Ann. Neurol.* **67,** 147–148 (2010).
18 Kurian, M. A., Morgan, N. V., MacPherson, L., Foster, K., Peake, D., Gupta, R. *et al.* Phenotypic spectrum of neurodegeneration associated with mutations in the PLA2G6 gene (PLAN). *Neurology.* **70,** 1623–1629 (2008).
19 Sina, F., Shojaee, S., Elahi, E. & Paisán-Ruiz, C. R632W mutation in PLA2G6 segregates with dystonia-parkinsonism in a consanguineous Iranian family. *Eur. J. Neurol.* **16,** 101–104 (2009).

THE JOURNAL OF BIOLOGICAL CHEMISTRY VOL. 286, NO. 52, pp. 44569–44575, December 30, 2011

Comparison of Presenilin 1 and Presenilin 2 γ-Secretase Activities Using a Yeast Reconstitution System*[S]

Received for publication, June 8, 2011, and in revised form, October 25, 2011 Published, JBC Papers in Press, November 10, 2011, DOI 10.1074/jbc.M111.270108

Yoji Yonemura[‡], Eugene Futai[‡1], Sosuke Yagishita[‡], Satoshi Suo[‡], Taisuke Tomita[§], Takeshi Iwatsubo[§], and Shoichi Ishiura[‡2]

From the [‡]Department of Life Sciences, Graduate School of Arts and Sciences, University of Tokyo, Tokyo 153-8902, Japan and the [§]Department of Neuropathology and Neuroscience, Graduate School of Pharmaceutical Sciences, University of Tokyo, Tokyo 113-0033, Japan

γ-Secretase is composed of at least four proteins, presenilin (PS), nicastrin (NCT), Aph1, and Pen2. PS is the catalytic subunit of the γ-secretase complex, having aspartic protease activity. PS has two homologs, namely, PS1 and PS2. To compare the activity of these complexes containing different PSs, we reconstituted them in yeast, which lacks γ-secretase homologs. Yeast cells were transformed with PS1 or PS2, NCT, Pen2, Aph1, and artificial substrate C55-Gal4p. After substrate cleavage, Gal4p translocates to the nucleus and activates transcription of the reporter genes *ADE2*, *HIS3*, and *lacZ*. γ-Secretase activity was measured based on yeast growth on selective media and β-galactosidase activity. PS1 γ-secretase was ~24-fold more active than PS2 γ-secretase in the β-galactosidase assay. Using yeast microsomes containing γ-secretase and C55, we compared the concentration of Aβ generated by PS1 or PS2 γ-secretase. PS1 γ-secretase produced ~24-fold more Aβ than PS2 γ-secretase. We found the optimal pH of Aβ production by PS2 to be 7.0, as for PS1, and that the PS2 complex included immature NCT, unlike the PS1 complex, which included mature NCT. In this study, we compared the activity of PS1 or PS2 per one γ-secretase complex. Co-immunoprecipitation experiments using yeast microsomes showed that PS1 concentrations in the γ-secretase complex were ~28 times higher than that of PS2. Our data suggest that the PS1 complex is only marginally less active than the PS2 complex in Aβ production.

γ-Secretase consists of at least four subunits, presenilin (PS),[3] nicastrin (NCT), anterior pharynx defective 1 (Aph1), and presenilin enhancer 2 (Pen2) (1). PS is the catalytic subunit of γ-secretase with aspartic protease activity (2, 3). Amyloid-β (Aβ) peptide, which plays a causative role in Alzheimer disease (AD), is produced after sequential cleavage of amyloid-β precursor protein (APP) by β-secretase and γ-secretase. The Aβ mainly consists of Aβ40 and Aβ42 containing 40 and 42 amino acids, respectively. Aβ42 is more prone to aggregation (4) and more toxic to neuronal cells. Many studies have reported that familial AD (FAD) mutations in PS and APP result in increased ratios of Aβ42 to Aβ40. The high Aβ42 ratio is believed to lead to AD.

PS has two homologs, namely, PS1 and PS2 (67% identical at the amino acid level). Aph1 also has two homologs: Aph1a (with alternative splicing variants Aph1a-S and a-L) and Aph1b. Sato *et al.* (5) reported that γ-secretase contained only one of each subunit, and as such, six distinct γ-secretases exist. Indeed, both PS1 and PS2 form a γ-secretase complex with the other subunits, producing Aβ (6). γ-Secretase cleaves many type I transmembrane proteins including APP and Notch, but the mechanism by which the different γ-secretases select their substrates is unclear. These different γ-secretases may have different functions and substrate selectivity.

Ubiquitous expression of PS1 and PS2 mRNAs in many human and mouse tissues has been reported, with varying expression levels across their tissues and during brain development (7). For example, in human young adult and aged brains, PS1 and PS2 mRNAs expression was similar. The subcellular distribution of PSs are known to be predominantly in the endoplasmic reticulum and the Golgi compartment (8). Levitan *et al.* (9) showed that human PS1 and PS2 substituted for *Caenorhabditis elegans* sel-12, suggesting that PS1 and PS2 are functionally redundant.

Different phenotypes of PS1- and PS2-deficient mice have been reported. PS1 knock-out mice exhibit severe developmental defects and perinatal lethality (10, 11), whereas PS2 knock-out mice show only mild phenotypes (12). Over 160 FAD mutations in PS1, but only 10 in PS2, have been found. These findings suggest that PS1 and PS2 play distinct roles *in vivo*.

Lai *et al.* (13) indicated that Ps1 (Ps, mouse presenilin) γ-secretase produced 169 times more Aβ than Ps2 γ-secretase, using membrane fractions from Ps1-(+/−), Ps2-(−/−), and Ps1-(−/−), Ps2-(+/+) blastocyst-derived cells from knock-out mice. In their study, γ-secretase activity was calculated as follows: level of produced Aβ/total Ps. They did not use the calculation: level of produced Aβ/Ps in γ-secretase complex and thus did not evaluate the active γ-secretase content.

Yagishita *et al.* (14) developed a novel γ-secretase assay using yeast microsomes. Yeast lacks endogenous γ-secretase and

* This work was supported in part by grants from Human Frontier Science Program and The Ministry of Health, Labor and Welfare, Japan.
[S] The on-line version of this article (available at http://www.jbc.org) contains supplemental Fig. S1.
[1] Present address: Dept. of Molecular and Cell Biology, Graduate School of Agricultural Science, Tohoku University, Sendai, Miyagi 981-8555, Japan.
[2] To whom correspondence should be addressed: 3-8-1 Komaba, Meguro-ku, Tokyo 153-8902, Japan. Tel. and Fax: 81-3-5454-6739; E-mail: cishiura@mail.ecc.u-tokyo.ac.jp.
[3] The abbreviations used are: PS, presenilin; APP, amyloid precursor protein; Aβ, amyloid β peptide; Aph1, anterior pharynx 1; CHAPSO, 3-[(3-cholamidopropyl)dimethylammonio]-2-hydroxy-1-propanesulfonic acid; CTF, carboxyl-terminal fragment; NCT, nicastrin; NTF, amino-terminal fragment; PC, phosphatidyl choline; Pen2, presenilin enhancer 2; FAD, familial Alzheimer disease; TM, transmembrane domain.

APP homologs, and one can reconstitute pure human γ-secretase in yeast and estimate the activity. Using this system, we compared the activity of PS1 and PS2 in γ-secretase complexes. Our data suggested that PS1-containing microsomes had much higher activity than PS2-containing microsomes. However, detailed analysis regarding the "active" γ-secretase complex revealed that the PS1 and PS2 complex produced similar levels of Aβ.

MATERIALS AND METHODS

Construction of γ-Secretase and Substrates—To reconstitute γ-secretase in yeast, human PS1 or PS2, NCT, Aph1a-L-HA, FLAG-Pen2, and substrates were cloned into the following vectors, as described previously (15). Briefly, PS1 or PS2 and NCT were ligated into KpnI and XbaI sites of the pBEVY-T vector (16). Aph1a-L-HA and FLAG-Pen2 were ligated into the XbaI and KpnI sites of pBEVY-L (16). C55-Gal4p, NotchTM-Gal4p, and C99 were fused to the *SUC2* signal sequence, facilitating translocation to the endoplasmic reticulum, and ligated into the BamHI and EcoRI sites of p426ADH (17). C55, C99, and NotchTM indicate amino acids 672–726 of the human APP770 isoform, 672–770 of the human APP770, 1703–1754 of the mouse Notch-1, respectively.

Myc-tagged PS1 and PS2 were PCR amplified and ligated into the KpnI site of pBEVY-T, using the following two pair of primers, respectively: mycPS1S, 5′-GGGGTACCAAAAATGGAACAAAAACTCATCTCAGAAGAGGATCTGATGACAGAGTTACCTGCACCGTTG-3′ and PS1AS, 5′-GATCCGCTTATTTAGAAGTGTCGAATTCGACCTCGGTACCATGCTAGATATAAAATTGATGGAATGC-3′; mycPS2S, 5′-GGGGTACCAAAAATGGAACAAAAACTCATCTCAGAAGAGGATCTGATGCTCACATTCATGGCCTCTGAC-3′ and PS2AS, 5′-GGGGTACCTCAGATGTAGAGCTGATGGGAGG-3′.

Yeast Transformation—Three plasmids were transformed into *Saccharomyces cerevisiae* strain PJ69–4A (*MATa, trp1–901, leu2–3, 112, ura3–52, his3–200, gal4Δ, gal80Δ, LYS2::GAL1-HIS3, GAL2-ADE2, met2::GAL7-lacZ*) (18). The transformants were selected on SD media plate lacking Leu, Trp, and Ura (SD-LWU). In microsome assays, we used the yeast strain PJ69–4Apep4Δ(*MATa, trp1–901, leu2–3, 112, ura3–52, his3–200, gal4Δ, gal80Δ, LYS2::-GAL1-HIS3, GAL2-ADE2, met2::GAL7-lacZ, pep4::kanMX*) (14) to avoid endogenous protease activity.

Reporter Gene Expression—Expression of *HIS3* (His) and *ADE2* (Ade) was estimated by transformant growth on SD-LWHUAde. β-Galactosidase assays were performed as described previously (15). Transformants were cultured in SD-LWU media until they reached an A_{600} of ~0.8. Cells were collected after centrifugation and suspended in lysis buffer (20 mM Tris-Cl (pH 8.0), 10 mM $MgCl_2$, 50 mM KCl, 1 mM EDTA, 5% glycerol, 1 mM dithiothreitol) including protease inhibitor mixture (Sigma), and lysed by glass beads. Protein concentration and β-galactosidase activity of the cell lysates were determined.

γ-Secretase Assay and Immunoblotting—Using yeast microsomes, we detected Aβ using an in vitro γ-secretase assay. *In vitro* γ-secretase assays were performed as described previously, with minor modifications (14). Microsomes (80 μg) were solubilized with γ-buffer (50 mM MES (pH 5.5) or 50 mM PIPES (pH 6.0, 6.5, 7.0, 7.5), or 50 mM HEPES (pH 8.0), 250 mM sucrose, 1 mM EGTA) containing 1% CHAPSO on ice for 60 min. Inhibitor mixture, thiorphan, *O*-phenanthroline, CHAPSO, and γ-buffer were added to the solubilized microsomes, as described previously (14). The mixture was incubated at 37 °C for 0 or 24 h. After incubation, the sample was extracted with chloroform/methanol (2:1) followed by addition of sample buffer, and boiled at 100 °C for 5 min. Aβ production was analyzed by Western blotting using the specific antibody, 82E1. Band signal was quantified using an LAS-3000 luminescent image analyzer (FujiFilm, Tokyo, Japan).

Immunoprecipitation of γ-Secretase—Microsomes (400 μg) were solubilized with IP buffer containing 1% CHAPSO and protease inhibitor mixture, on ice, for 60 min. Solubilized membranes were added to 40 μl of anti-FLAG affinity gel (50% slurry) (Sigma) and rotated at 4 °C for 2 h. Beads were washed with IP buffer and suspended in sample buffer containing 8 M urea to prepare the "IP sample" from 400 μg of microsomes. The "input sample" was prepared as follows: 100 μl of sample buffer containing 8 M urea was added to 80 μg of microsomes and incubated at 65 °C for 10 min. Microsomes (8 μg, 10–11 μl) were loaded as input.

Antibodies—The following antibodies were used for immunoblotting: monoclonal antibodies against Aβ, 82E1 (IBL, Fujioka, Japan), HA (12CA5; Sigma), FLAG (M2; Sigma), and polyclonal antibodies against NCT (AB5890; Chemicon, Temecula, CA), Myc, 2272 (Cell Signaling Technology, Beverly, MA), the PS1 loop region (G1L3) (19), and the PS2 loop region (G2L) (20).

RESULTS

PS2 Was Less Active than PS1 in Growth and β-Galactosidase Assays—We constructed recombinant plasmids for γ-secretase and APP-based (C55-Gal4p) or Notch-based substrates (NotchTM-Gal4p) (15). We introduced the vectors into yeast strain PJ69, which expresses *HIS3*, *ADE2*, and *lacZ* under Gal4p control, and generated yeast transformants expressing the γ-secretase subunits (PS1 or PS2, NCT, Aph1a-L-HA, FLAG-Pen2) and an artificial substrate (C55-Gal4p or NotchTM-Gal4p). Gal4p released from C55-Gal4p or NotchTM-Gal4p by reconstituted γ-secretase activates *HIS3* and *ADE2* genes transcription. Therefore, γ-secretase activity was assessed by growth on media lacking histidine and adenine. As a result, yeast expressing PS1 γ-secretase and C55-Gal4p could replicate on the selection media. Yeast expressing PS2 γ-secretase could also grow, but was much slower than that of PS1-expressing yeast (Fig. 1*A*). PS1 L166P, G384A, and PS2 N141I are familial Alzheimer disease (FAD) mutations. Yeast carrying these mutations were unable to grow on media lacking histidine and adenine. After isolating these yeast cell lysates, we measured β-galactosidase activity to estimate γ-secretase activity. PS1 had ~24 times more β-galactosidase activity than PS2 (Fig. 1*B*). The results of the β-galactosidase assay were well correlated with the growth assay results (Fig. 1, *A* and *B*).

Next, we used NotchTM-Gal4p as a substrate instead of C55-Gal4p. The results were similar to those obtained when using

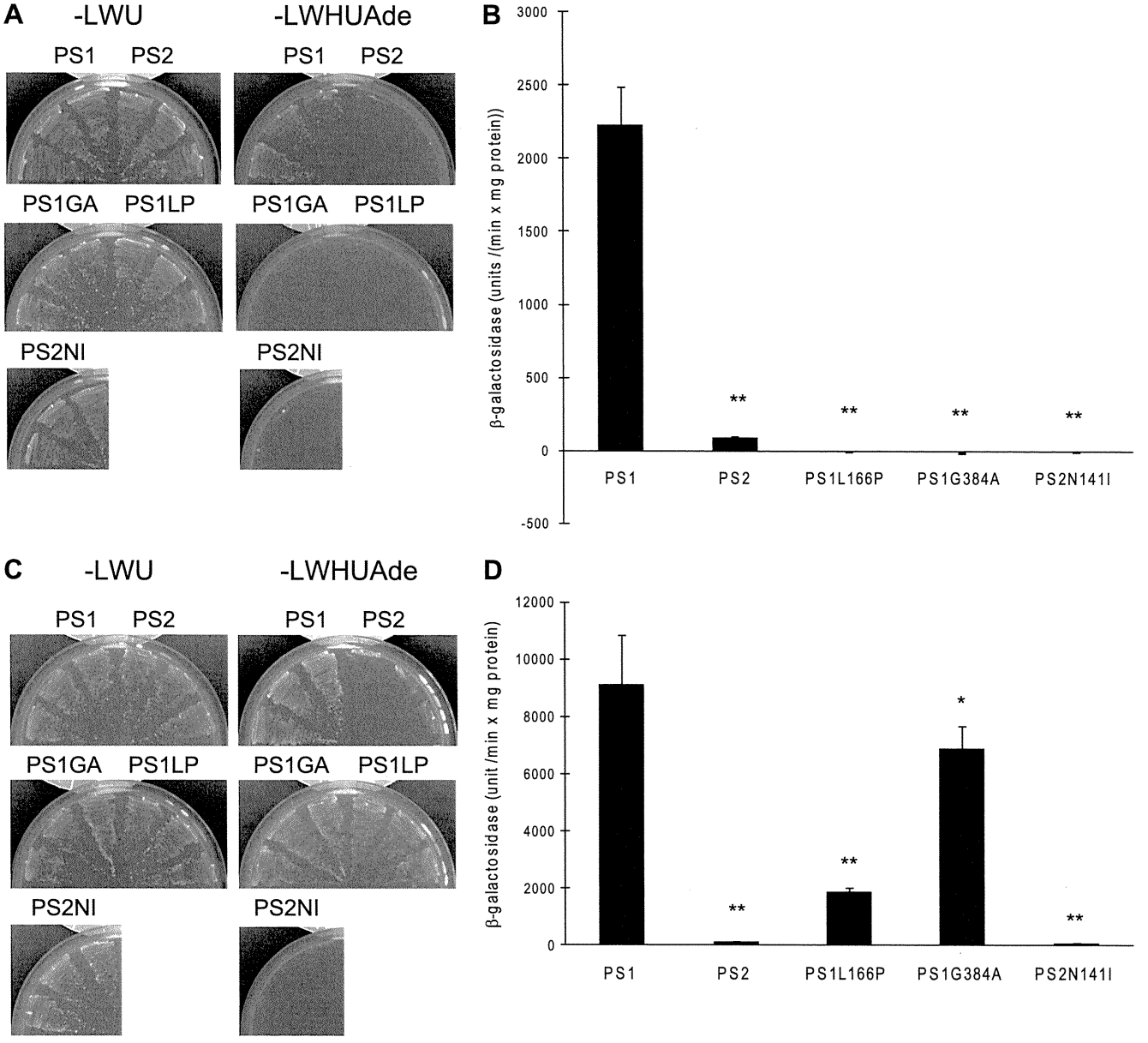

FIGURE 1. **Estimate of reconstituted PS1 or PS2 γ-secretase activity in yeast.** *A* and *C*, yeast cells were transformed with PSs (PS1 or PS2, or PS with FAD mutations), NCT, FLAG-Pen2, Aph1a-L-HA, and C55-gal4p (*A*), or NotchTM-gal4p (*C*). Three independent clones were cultured on non-selection media (SD-LWU) or selection media (SD-LWHUAde) at 30 °C for 3 days. Yeast cells not expressing PS did not grow on SD-LWHUAde. *B* and *D*, β-galactosidase activity was measured for each yeast lysate. Lysates were prepared from yeast cells using glass beads. One unit of β-galactosidase activity corresponds to 1 nmol of *O*-nitrophenyl β-d-galactopyranoside hydrolyzed per min, and activity was calculated as unit/(min × mg of protein in lysate). The activity was normalized by subtracting the activity in the absence of PS, 65 unit/(min × mg protein). Data are presented as mean value ± S.D., $n = 18$ (*A*), $n = 3$ (*C*) *, $p < 0.05$; **, $p < 0.01$ (analyzed by one-way analysis of variance followed by Dunnett's multiple comparison test). Statistical analyses were performed with PRISM software.

the C55-Gal4p, with the following two exceptions. Notch1 was more likely to be cleaved by γ-secretase than C55 (APP) (Fig. 1, *B versus D*) and yeast cells expressing PS1 with FAD mutations (L166P and G384A) were able to grow on SD-LWHUAde, whereas cells expressing PS2 N141I were not (Fig. 1*D*). These results suggested that PS1 with the FAD mutations cannot cleave APP, whereas they can cleave Notch like wild-type γ-secretase.

Optimal pH for Aβ Production by the PS2 Complex—To study γ-secretase activity *in vitro*, we prepared yeast microsomes from yeast transformants expressing PS1 or PS2, NCT, Aph1a-L-HA, FLAG-Pen2, and C55 (14). Three previous reports showed that γ-secretase with PS1 maximally produced Aβ at approximately pH 7.0 (14, 21, 22). The optimum pH of Aβ production by γ-secretase with PS2, however, remains unclear. Thus, we investigated the optimal pH of the PS2 complex to produce Aβ. When yeast microsomes prepared from three independent clones were incubated for 24 h at 37 °C with 0.25% CHAPSO and 0.1% PC, we found that the PS2 complex also maximally produced Aβ at approximately pH 7.0 in all three assays (Fig. 2, *A* and *B*), suggesting that the PS1 and PS2 complex have similar pH dependences for Aβ production.

Levels of Aβ Production by PS1 or PS2—We compared the level of Aβ produced by PS1 or PS2 using yeast microsomes. Each microsome was incubated at 37 °C for 24 h in the pres-

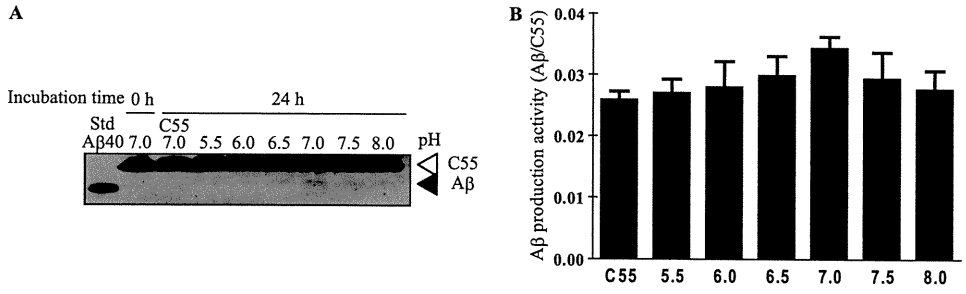

FIGURE 2. **Optimum pH of Aβ production by PS2.** *A*, microsomes (80 μg) prepared from three independent yeast cells transformed with PS2, NCT, Aph1a-L-HA, FLAG-Pen2, and C55, and from yeast expressing C55 were incubated with 0.25% CHAPSO and 0.1% PC at 37 °C for 0 or 24 h. Incubation samples were subjected to immunoblotting to compare Aβ production activity, Aβ/C55. Aβ was detected by 82E1. Synthetic Aβ40 (20 pg) was used as a positive control. Yeast expressing C55 and microsomes incubated for 0 h were loaded as a negative control. *B*, three independent assays were quantified using analyzing software (LAS-3000 luminescent image analyzer, Fuji Film, Tokyo, Japan). The column represents the mean ± S.D. ($n = 3$).

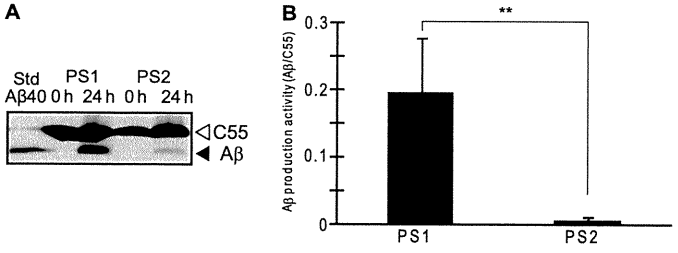

FIGURE 3. **Difference in Aβ production between PS1 and PS2.** *A*, yeast microsomes expressing PS1 or PS2, NCT, Aph1a-L-HA, FLAG-Pen2, and C55 were subjected to *in vitro* γ-secretase assays at pH 7.0. Aβ produced by PS1 or PS2 γ-secretase was detected. Synthetic Aβ40 (30 pg) was loaded as a marker. *B*, the bands obtained in *A* were quantified to determine the ratio of Aβ to C55 using analyzing software (LAS-3000 luminescent image analyzer, Fuji Film, Tokyo, Japan). The column represents the mean ± S.D. ($n = 5$, **, $p < 0.01$). Data were analyzed by Student's *t* test.

ence of 0.25% CHAPSO and 0.1% PC. We found that the PS1 complex produced significantly more Aβ than PS2 (Fig. 3*A*). By quantifying the Western blotting signals, we calculated that PS1 produced ~24 times more Aβ than PS2 (Fig. 3*B*).

PS1 Complexes Were More Abundant than PS2 Complexes—To verify whether PS, NCT, Aph1a-L, and Pen2 form the γ-secretase complex, we isolated membrane fractions from yeast introduced with PS, NCT, Aph1a-L-HA, FLAG-Pen2, and C99, and performed co-immunoprecipitation experiments with the anti-FLAG M2 affinity gel. Both PS1 and PS2 were co-immunoprecipitated with FLAG-Pen2 (Fig. 4, *B* and *C*). NCT and Aph1a-L were also co-immunoprecipitated with FLAG-Pen2 (Fig. 4*A*), suggesting that PS1 and PS2 formed a γ-secretase complex. We also found that the PS2 complex predominantly included non-glycosylated immature NCT, whereas the PS1 complex contained highly glycosylated mature NCT (Fig. 4*A*).

Comparison of the PS1 and PS2 contents in γ-secretase is difficult due to the variable affinity of their specific antibodies. To estimate the amount of PS1 or PS2 in γ-secretase complexes, we constructed Myc-tagged PS1 and PS2. We introduced these constructs into yeast and reconstituted the γ-secretases. Preparing these microsomes, we immunoprecipitated γ-secretase complexes with anti-FLAG affinity gel. The immunoprecipitates were next subjected to immunoblotting. Aph1a-L levels in the PS1 or PS2 complex were similar (Fig. 5*A*). The Myc-tagged PS1 complex included mainly mature NCT, while Myc-tagged PS2 complexes contained immature NCT (Fig. 5*A*). The level of PS1 NTF in γ-secretase complexes (associated with FLAG Pen2) was ~28 times higher than that of PS2 NTF (Fig. 5*B*).

When calculating γ-secretase activity per one γ-secretase complex from these data, a significant difference between PS1 and PS2 does not exist. However, the PS1 complex was 24.15 more active in the β-galactosidase assay. *In vitro* Aβ production assays indicated that PS1 was 24.61 more active than PS2. Comparing PS1 and PS2 contents in γ-secretase in a co-immunoprecipitation experiment, we found that the amount of PS1NTF in the γ-secretase complex was 28.14 times higher than that of PS2NTF. These data suggested that the complete PS2 complex was 1.142 or 1.143 times more active than the PS1 complex.

DISCUSSION

γ-Secretase assays measuring released Aβ into conditioned media from cultured cells have been previously performed. These assays found that γ-secretase with PS FAD mutations increased the Aβ 40/42 ratio. However, very few *in vitro* assays have been reported. To accurately study γ-secretase activity, Yagishita *et al.* (14) established an *in vitro* assay system using yeast, which possesses no γ-secretase homologs. This system enabled us to directly compare activities between the PS1 and PS2 complex.

Yeast growth and β-galactosidase assays using C55-Gal4p or Notch-Gal4p as a substrate revealed that PS1 had a significantly higher activity than PS2. We also found that FAD mutations in PS abolished APP processing activity, and that PS1 L166P and G384A cleaved Notch with reduced activity compared with wild-type PS1. The assembly of PS1 FAD mutants (L166P or G384A) into γ-secretase complex was also assessed by immunoprecipitation (supplemental Fig. S1). The assembly of PS1 L166P mutant was similar to PS1 WT. On the other hand, ~36% of PS1 G384A (comparing to the WT) formed the γ-secretase complex. These results showed that PS1 L166P assembled normally with defective protease activity and PS1 G384A was defective both in the assembly and the protease activity, suggesting that loss of function of PS caused lower cleavage activity. These reductions in processing activity obtained in this report support PS loss of function hypothesis, which is believed to cause FAD (23). We evaluated the activity of other PS1 FAD mutations (A79V, M146L, A231V, M233T, and ΔExon9) in Notch cleavage (data not shown). Our Notch

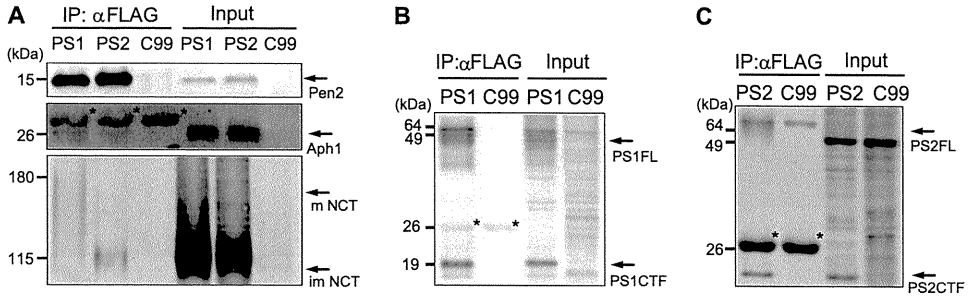

FIGURE 4. **Formation of PS1 and PS2 γ-secretase complexes.** Yeast microsomes expressing PS1 or PS2, NCT, Aph1a-L-HA, FLAG-Pen2, and C99, and microsomes expressing C99 were solubilized with IP buffer containing 1% CHAPSO and protease inhibitor mixture. γ-Secretase complexes were immunoprecipitated with anti-FLAG affinity gel (Sigma). The immunoprecipitates and input fraction were subjected to immunoblotting. NCT, Aph1, Pen2, and PS were detected by specific antibodies. The *asterisks* indicate nonspecific bands.

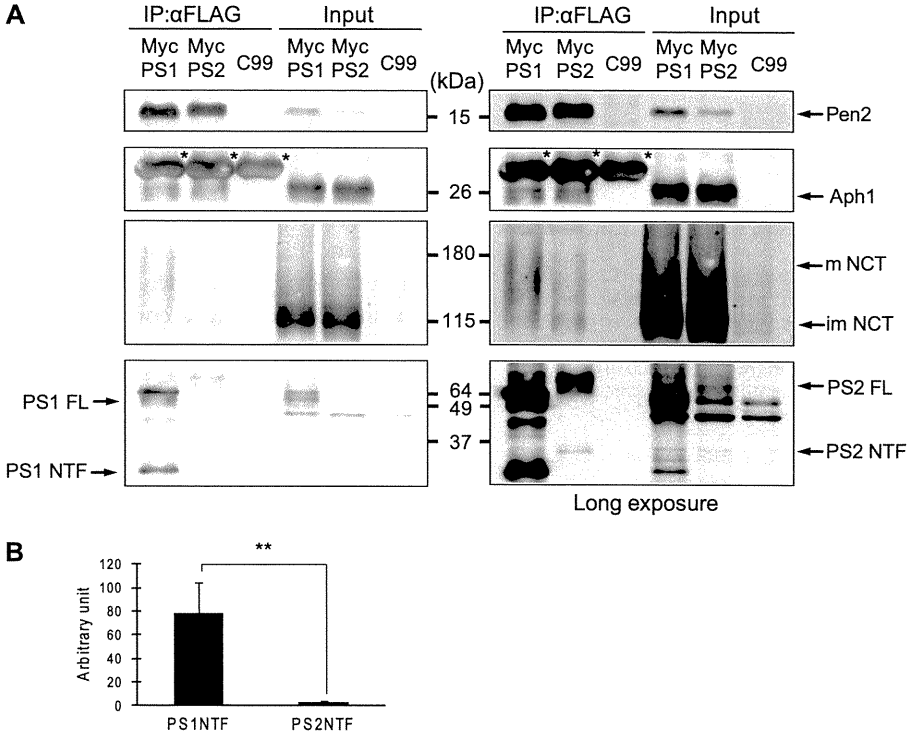

FIGURE 5. **Quantification of PS1 and PS2 in γ-secretase complexes.** *A*, yeast expressing Myc-tagged PS1 or PS2, the other secretase subunits, and C99, were incubated with anti-FLAG affinity gel. The immunoprecipitates were analyzed by immunoblotting. *B*, amount of Myc-tagged PS1NTF and Myc-tagged PS2NTF in the γ-secretase complexes were quantified using LAS-3000 luminescent image analyzer (Fuji Film, Tokyo, Japan). Data were analyzed by Student's *t* test. Error bar shows the mean ± S.D. $n = 4$, **, $p < 0.01$. The *asterisks* indicate nonspecific bands.

cleavage results with PS1 FAD mutations, PS1L166P and G384A, corroborated the findings of earlier studies (24, 25).

Based on the *in vitro* γ-secretase assay using yeast microsomes, we found that γ-secretase with PS2 optimally produced Aβ at approximately pH 7.0. Previous reports have shown that PS1 also maximally produced Aβ at pH 7.0 (14, 21, 22), suggesting that PS1 and PS2 make Aβ using a similar mechanism.

Our co-immunoprecipitation experiments using yeast microsomes containing PS1 or PS2, NCT, Aph1a-L-HA, and FLAG-Pen2 showed that PS2 bound to immature NCT, whereas PS1 bound to the mature NCT. Expression levels of immature or mature NCTs in cells transformed with PS1 or PS2 were similar, but the anti-FLAG affinity gel immunoprecipitates contained different levels of immature and mature NCT. Frånberg *et al.* (26) reported that Ps2 bound to immature NCT in Ps1-deficient (Ps1-(−/−), Ps2-(+/+)) MEF cells and Ps1 bound to mature NCT in Ps2 deficient (Ps1-(+/+), Ps2-(−/−)) MEF cells using affinity capture with an active site-directed γ-secretase inhibitor. This difference in NCT maturation in the complex may affect substrate affinity.

In this study, we used Aph1a-L as a γ-secretase subunit, which may facilitate PS2 binding to immature NCT. Also, Aph1a-S expression, or Aph1b as a γ-secretase subunit, may result in alternative binding patterns, such as PS2 binding to mature NCT or PS1 binding with immature NCT. In fact, we observed the PS1 complex with Aph1a-S containing more immature NCT than the PS1 complex with Aph1a-L (data not shown). To date, γ-secretase is known to target many substrates, but how γ-secretase selects its substrates is unclear. These variable γ-secretases may contribute to specific substrate selection.

To compare the γ-secretase activity of PS1 and PS2 precisely, we employed two different approaches. First, we used C55(-Gal4p) or C99 as a substrate instead of C100Flag. NCT